Geochronology of metamorphic events in the lower crust beneath NW Russia: a xenolith Hf isotope study

Marina Koreshkova[1]*, Hilary Downes[2], Ian Millar[3], Lev Levskii[4], Aleksandr Larionov[5] and Sergey Sergeev[5]

[1]Institute of Earth Sciences, St Petersburg State University, St Petersburg 199034, Russia, [2]Department of Earth and Planetary Sciences, Birkbeck University of London, London WC1E 7HX, UK,

[3]NERC Isotope Geoscience Laboratory, Keyworth NG12 5GG, UK,

[4]Institute of Precambrian Geology and Geochronology, Russian Academy of Sciences, St Petersburg 199034, Russia, and [5]Isotope Research Centre, VSEGEI, St Petersburg 199106, Russia

*Corresponding author: Telephone +7812 3636201. E-mail: m.koreshkova@spbu.ru

ABSTRACT

Hf isotope data for zircons and whole-rocks from lower crustal mafic granulite and pyroxenite xenoliths from NW Russia are presented together with the results of U-Pb zircon dating, Sm-Nd and Rb-Sr isotopic compositions of bulk-rocks and minerals, and trace element compositions of minerals. Most zircons only preserve a record of the youngest metamorphic events, but a few Grt-granulite xenoliths retain Archean magmatic zircons from their protolith. Metamorphic zircons have highly variable εHf(t) values from -25 to -4. The least

radiogenic zircons were formed by recrystallization of primary magmatic Archean zircons. Zircons with the most radiogenic εHf grew before garnet or were contemporaneous with its formation. Zircons with εHf(t) from -15 to -9 formed by various mechanisms, including recrystallization of pre-existing metamorphic zircons, subsolidus growth in the presence of garnet and exsolution from rutile. They inherited their Hf isotopic composition from clinopyroxene, pargasite, rutile and earlier-formed zircon which had equilibrated with garnet. Subsolidus zircons were formed in response to a major change in mineral association, i.e., garnet- and zircon-producing reactions including partial melting. Recrystallized zircons date the onset of high temperature conditions without a major change in mineral association. Age data for metamorphic zircons fall into five groups: >1.91 Ga, 1.81-1.86 Ga, 1.74-1.77 Ga, 1.64-1.67 Ga and <1.6 Ga. Most ages correlate with metamorphic events in the regional upper crust superimposed onto rocks of the Belomorian belt during formation of the Lapland Granulite Belt. Zircon formation and re-setting at 1.64-1.67 Ga significantly postdates Lapland-Kola orogenic events and may relate to the onset of Mesoproterozoic rifting. The youngest ages (1.6-1.3 Ga) correspond to an event that affected only a few grains in some samples and can be explained by interaction with a localized fluid. The observed garnet-granulite associations were formed 1.83 Ga ago in Arkhangelsk xenoliths and 1.74-1.76 Ga ago in most Kola xenoliths. By the end of the Lapland-Kola orogeny, the rocks were already assembled in the lower crust. However, no addition of juvenile material has been detected and preservation of pre-Lapland-Kola metamorphic zircon indicates that some xenoliths represent an older lower crust. Granulites, pyroxenites and Phl-rich rocks have a common metamorphic history since at least ca 1.75 Ga. At about 1.64 Ga metasomatic introduction of phlogopite took place; however, this was only one of several phlogopite-forming events in the lower crust.

Key words: lower crust, xenoliths, zircon, Hf isotopes; Kola Peninsula

INTRODUCTION

Understanding the metamorphic history of the lower continental crust is important in order to evaluate the age of assembly of rocks of possible different origins, and to establish whether there was a single event of lower crust formation or several periods. Dating of lower crustal rocks also helps to determine the timing of compositional changes in the lower crust such as depletion caused by partial melting or re-enrichment related to metasomatism. However, mineral associations in lower crustal xenoliths from beneath Precambrian areas are usually well-equilibrated and, or, have experienced slow cooling, and so rarely preserve evidence of earlier metamorphic events. In the absence of other data, information obtained from zircon is the most important tool to investigate the geological history of lower crustal xenoliths and to place constraints on the age and origin of their protoliths. A combination of zircon morphology, composition, geochronology and Hf isotopic composition can shed light on these issues. Since Hf is a major constituent of zircon, Hf isotope ratios of dated zones in zircons can also yield information about the lower crust and the events recorded within it.

Lower crustal xenoliths in Devonian alkaline dikes and pipes of the Kola Peninsula and the Arkhangelsk kimberlite province of NW Russia are fragments derived from beneath the late Archean Belomorian Mobile Belt. They have been previously studied for their mineralogy, petrology and Nd-Sr isotopic composition (Vetrin & Kalinkin, 1992; Kempton *et al*., 1995, 2001; Markwick & Downes 2000; Koreshkova *et al*., 2001) and U-Pb zircon ages (Downes *et al*., 2002; Vetrin *et al*., 2009; Koreshkova *et al*., 2014). These data pose several important questions: the reason for the spread of Proterozoic concordant U-Pb zircon ages, the

significance and geological meaning of ages younger than 1.75 Ga (the age of the youngest events in the regional upper crust), and the origin of Archean zircons.

This study combines data on the texture, composition, mineral relationships and Hf isotopic composition of zircons from lower crustal xenoliths from the Kola Peninsula and Arkhangelsk, in order to determine the source and mechanisms of zircon formation. Interpretation of age and Hf isotope data allow reconstruction of the timing of metamorphic events in the lower crust beneath the Belomorian Mobile Belt.

GEOLOGICAL BACKGROUND AND PREVIOUS GEOCHRONOLOGICAL STUDIES

Samples from the Kola Peninsula were collected from olivine melilitite dikes and a diatreme on the Elovy and Salny islands in the White Sea, near Kandalaksha, which are part of the Devonian Kola alkaline province (Beard *et al*., 1996). Those from the Arkhangelsk kimberlite province (Beard *et al*., 2000; Makhotkin *et al*., 2000) were obtained from drill core from the Grib kimberlite pipe. The local basement rocks of both areas belong to the late Archean Belomorian Mobile Belt, in close proximity to the early Proterozoic Lapland belt between the Kola composite terrane and Karelian craton (Fig. 1). The Kandalaksha dikes intrude migmatites of the Khetolambina nappe (Glebovitsky, 1997; Bibikova *et al*., 2004). The basement of the Arkhangelsk area is covered by Neoproterozoic and Late Palaeozoic sediments. However, Samsonov *et al*. (2009) reported Proterozoic Nd model ages for basement rocks from boreholes in the central part of the Arkhangelsk province, and Archaean ages from the northern and southern parts.

Thermal Ionisation Mass Spectrometry (TIMS) analyses on single zircon grains from one Kola lower crustal granulite xenolith were reported by Vetrin & Nemchin (1998) and yielded an age of 1729±29 Ma. Zircons from two Kola xenoliths, previously studied for their

petrology and geochemistry by Kempton *et al*. (1995, 2001), were dated by Downes *et al*. (2002) by ion microprobe (NORDSIM); these gave ages of 2.84 and 2.47 Ga for magmatic zircons and 1.77-1.45 Ga for metamorphic ones. The oldest age (2.84 Ga) comes from a single grain and was interpreted as inherited. The 2.47 Ga value was compared to widespread early Proterozoic magmatism; thus the xenoliths could be the deep-seated equivalents of Large Igneous Province basalts. The ages around 1.7 Ga were ascribed to migmatization and may be related to local emplacement of pegmatites. Vetrin *et al*. (2009) reported U-Pb zircon ages from 2788 to 261 Ma, the younger values clearly demonstrating contamination during zircon separation, being younger than the host magma age. Zircon data for four Grt-granulite xenoliths combined to give a cluster at 2788±35 Ma (two grains with concordant age), a cluster of discordant grains with an upper intercept at 2837±26 Ma, and a series of concordant ages from 1770 to 1440 Ma. Ages corresponding to the Lapland orogeny (1.95-1.80 Ga) are missing in the Kola xenoliths, but are preserved in those from Arkhangelsk (Koreshkova *et al*., 2014). In general, these data show that careful investigation of zircon origin is necessary for correct interpretation of zircon ages in such xenoliths.

ANALYTICAL TECHNIQUES AND SAMPLES

For this study we selected five Grt-granulite xenoliths (Mk111, Mk260, Mk325, Mk326 and Mk523), a Grt-websterite (Mk459), a Prg-Phl-eclogite (Mk284), two Phl-rich, Grt-bearing rocks (Mk172 and Mk540) and a Phl-Prg-clinopyroxenite (Mk536) from Kola, and three Grt-granulites from Arkhangelsk (P5/354, 60/473 and 77/690). Abbreviations for rock-forming minerals are: Cpx – clinopyroxene, Grt – garnet, Opx – orthopyroxene, Phl – phlogopite, Pl – plagioclase, Prg – pargasite, Qtz – quartz, Zrn – zircon and others according to Kretz (1983). We report new data for sample Mk111 (studied previously by Koreshkova *et al.* (2001)). The

petrographic, mineralogical and zircon dating results for the Arkhangelsk samples were published by Koreshkova *et al*. (2014).

Polished thin sections were used for petrographic descriptions, electron microprobe (EMP) and Laser Ablation Inductively Coupled Plasma Mass Spectrometry (LA-ICP-MS) analyses. Modal mineralogy was estimated using an integration stage and "ImageScope" software (Table 1). Detailed descriptions of samples from the Kola Peninsula are given in Supplementary Data Electronic Appendix 1 (http://www.petrology.oxfordjournals.org). Bulk-rock analyses for major (X-ray Fluorescence (XRF)) and trace elements (Solution Inductively Coupled Plasma Mass Spectrometry (ICP-MS)) were obtained at VSEGEI (St Petersburg) for the granulites and a Phl-Grt-Opx rock Mk174 which is analogous to samples Mk540 from this study and 436-11 studied by Kempton *et al.* (2001) (Supplementary Data Electronic Appendix 2). Grt-websterite Mk459 is similar to the samples described by Koreshkova *et al*. (2001) and Kempton *et al*. (2001), Mk180 and 436-17, respectively.

Major element analyses of minerals were obtained using a JEOL 8100 Superprobe at Birkbeck/UCL. Data for the Kola samples are reported in Supplementary Data Electronic Appendices 3a and 3b. Data for the Arkhangelsk samples were previously published by Koreshkova *et al*. (2014).

Trace element analyses of constituent minerals were made at Birkbeck using a New Wave Research UP213 laser aperture imaged frequency quintupled Nd:YAG solid state laser operating at 213 nm, coupled to an Agilent 7500a quadrupole ICP-MS. Data obtained for minerals from the Kola samples and analyses of standards are reported in Supplementary Data Electronic Appendices 4a-c. The results of the study of mineral compositions and zoning in garnet and pyroxenes from the Kola xenoliths are presented in Supplementary Data Electronic Appendix 5. Analyses of zircons are shown separately in Electronic Appendix 6. For Arkhangelsk xenoliths, we report only new data on garnet and rutile from sample 77/690.

Brief characteristics of the textures and compositions of the Arkhangelsk zircons are given in the section "*Hf isotope composition of zircon*".

Results of U-Pb dating using SHRIMP (St Petersburg) of zircons from xenoliths Mk111, Mk172, Mk260, Mk284, Mk325, Mk326, Mk459 and Mk523 are given in Supplementary Data Electronic Appendix 7. Laser-ICP-MS dating of zircons in thin section was undertaken at Birkbeck/UCL on two samples Mk540 and Mk536 (Supplementary Data Electronic Appendix 7).

Lu-Hf data were obtained for zircons from samples Mk111, Mk326, Mk523, Mk172, Mk284 and Mk459 from Kola and samples 60/473, P5/354 and 77/690 from Arkhangelsk. Zircons from samples Mk260 and Mk325 were too small to be analyzed. Lu-Hf data for samples and standards are reported in Table 3. Isotope analyses were carried out at NIGL using a Thermo Scientific Neptune Plus MC-ICP-MS coupled to a New Wave Research UP193FX Excimer laser ablation system and a low-volume ablation cell. Bulk-rock Hf isotope data were obtained for five Kola Grt-granulites previously studied by Kempton *et al.* (1995, 2001) and are presented in Table 3.

Sm-Nd and Rb-Sr isotope analyses were undertaken on whole-rock samples (Mk111, Mk260 and Mk284) and separated minerals (garnet, clinopyroxene, amphibole and mica) from the listed samples and 77/690 at the IPGG (St Petersburg). The data are reported in Supplementary Data Electronic Appendix 9.

Detailed descriptions of the analytical techniques used are given in Supplementary Data Electronic Appendix 10.

RESULTS

Petrography

Grt-granulite xenoliths from Kola have typical medium- to coarse-grained, foliated or banded structure and porphyroblastic texture. They contain garnet, clinopyroxene, plagioclase and minor orthopyroxene, quartz, orthoclase, phlogopite, pargasite and scapolite (Table 1, Supplementary Data Electronic Appendix 1). The presence of orthopyroxene in Mk260 reflects its high-magnesium bulk-rock composition (13.6 wt % MgO). Sample Mk459 is a metamorphic rock composed of garnet and two pyroxenes and is termed Grt-websterite throughout the text. These Grt-websterites share many common features with the granulites. They are similar in texture, composition of minerals, P-T conditions of metamorphism and zircon age (see section "*Zircon ages and their significance*"). Phl-rich eclogite Mk284 is a coarse-grained, foliated, porphyroblastic rock containing omphacite, pyrope, pargasite and phlogopite. However, the compositions of its constituent minerals do not differ significantly from those in the granulites. Samples of this type are uncommon and might represent fragments of lowermost crust or uppermost mantle. Phlogopite is in reaction relationship with clinopyroxene and shows a preferred orientation and deformation bands in all samples. Sometimes reaction relationships are obscured by superimposed deformation and recrystallization. Phlogopite also replaces garnet and orthopyroxene in sample Mk540, which is analogous to 436-11 studied by Kempton *et al.* (1995). Sample Mk172 is small and unrepresentative, but similarities in garnet and zircon compositions indicate an affinity to Mk540 and other Phl-Grt-Opx rocks. This sample demonstrates an ultimate degree of replacement by phlogopite. Phl-clinopyroxenite Mk536 is a medium-grained, foliated, granoblastic rock. Its analogue was found in contact with granulite in a composite xenolith, which implies that these pyroxenites belong to the lower crustal assemblage. Like other samples, it shows signs of plastic deformation in the rock-forming minerals.

Samples from Kola show minor alteration, unlike those from Arkhangelsk which are strongly altered (Koreshkova *et al*., 2014). The characteristics of the mineral compositions

and zoning in garnet and pyroxenes from the Kola xenoliths are presented in Supplementary Data Electronic Appendix 5. We have included estimates of the P-T conditions for the Kola samples using the formulations of the Grt-Cpx geothermometer of Ravna (2000), the Zr-in-rutile geothermometer of Watson *et al.* (2006), the Grt-Pl-Cpx-Qtz geobarometer of Newton & Perkins (1982) for granulites and the Grt-Opx geobarometer of Nickel & Green (1985) (modified version by Taylor (1998)) for pyroxenites in Table 1. We consider that temperatures obtained from the Zr content in rutile reflect better the peak conditions at the time of formation of the mineral associations. The zoning in garnet and pyroxene grains (Supplementary Data Electronic Appendix 5 and section "*Mineral compositions and zoning*") suggest that their cores could be out of equilibrium, whereas their rim compositions might correspond to equilibration during final cooling. Thermobarometric estimates demonstrate higher P-T conditions for the Kola samples (700-930^{o}C, 1.2-1.5 GPa; Kempton *et al*., 1995; this study) compared to those from Arkhangelsk (670-800°C, 1.0-1.2 GPa, Markwick & Downes, 2000; Koreshkova *et al*., 2014).

Generally, the Grt-granulites have basalt-like bulk-rock compositions. The granulites are LREE-enriched and have negative Nb and positive Pb anomalies. Eclogite Mk284 is characterized by strongly elevated incompatible element contents, especially Rb, Ba, Nb and Ta. Phl-Grt-Opx rocks have flat REE patterns with strong negative Eu anomalies (Supplementary Data Electronic Appendix 2). Phl-Grt-Opx rocks and the Phl-clinopyroxenite Mk536 might represent metamorphosed cumulative pyroxenites.

U-Pb dating of zircons from the Kola samples, their textures in CL and compositions

Grt-granulite Mk111

Grt-granulite Mk111 contains numerous pink zircons which are rounded to polygonal and faceted. About 135 grains were mounted in three grain-mounts according to their size: 230-620 μm, 110-340 μm and 90-210 μm. Five major textural types were recognized in CL: fir-tree sector-zoning, CL-dark polygonal sector-zoning, bright homogeneous, patchy, and convoluted overgrowths which are responsible for the polygonal shape (Fig. 2a). Patchy texture, polygonal and fir-tree sector-zoning are observed with equal frequency (about 30%) within grain cores. Bright homogeneous shells on the cores are mostly thin and discontinuous; completely homogeneous grains occur rarely (6%). About 40% of grains have convoluted overgrowths. Patchy texture represents disturbed textures of other types. It is probably caused by the development of darker in CL stripes and rims. The rims are better seen on homogeneous grains (Fig. 2a).

CL-dark, sector-zoned cores are characterized by low Th/U (and high U), low REE contents and negative REE slopes (Fig. 3a). Fir-tree zircons have much higher REE, Y and Th contents, relatively high Th/U (1.6-3.8), moderate HREE slopes (Yb_N/Dy_N = 2.1) and negative Eu-anomalies. These zircons contain inclusions of orthopyroxene which is absent from the groundmass. Homogeneous, CL-bright grains show similar REE patterns but with lower REE concentrations and low Th and U contents. Overgrowths have lower REE contents, shallower HREE slopes and smaller negative Eu anomalies in comparison to homogeneous zircons. The composition of patchy zircons and outer rims varies significantly, but the rims clearly show elevated Th contents with Th/U about 6.7. Some discrepancies in Th and U concentrations determined by LA-ICP-MS and SHRIMP result from differences in sampling volumes.

The oldest age (2252 Ma from $^{207}Pb/^{206}Pb$) was obtained from one CL-dark polygonal sector-zoned grain. Younger ages of 1864-1482 Ma from $^{207}Pb/^{206}Pb$, obtained from three other grains, can be the result of re-setting. Fir-tree zircons show $^{207}Pb/^{206}Pb$ ages between

1931 and 1849 Ma, except for one grain with blurred zoning that gave a value of 1776 Ma (Fig. 5a). CL-bright homogeneous zircons yielded $^{207}Pb/^{206}Pb$ ages of 1868, 1853 and 1764 Ma. Overgrowths analyzed by SHRIMP show elevated Th/U similar to CL-dark outer rims. We suggest that these overgrowths were affected by CL-dark rim formation, probably due to diffusional exchange. The overgrowths and rims together show $^{207}Pb/^{206}Pb$ ages of 1706-1794 Ma.

The data can be divided into 5 age groups. The first comprises a single grain with an age of 2252 Ma (or older because we cannot exclude partial re-setting). Most zircons fall into three groups of concordant ages: 1918±31 Ma, 1859±13 Ma and 1759±18 Ma (Fig. 5a). Two grains with ages <1.7 Ga form the fifth group. The five metamorphic zircon generations were formed in the course of distinct metamorphic events, as follows from the difference in zircon textures and compositions and inferred changes of mineral associations. Each subsequent event could cause a partial or complete re-setting of the Th-U-Pb system in previously formed zircons, taking into account the high temperature of metamorphism and the evidence for multiple heating events. We suggest that the oldest age shown by zircon of one generation is the best approximation to the age of a metamorphic event. Consequently CL-dark zircons with polygonal sector-zoning were formed 2.25 Ga ago or earlier, sector fir-tree zoned zircons formed 1918±31 Ma ago, bright homogeneous zircons formed 1859±13 Ma ago, and the convoluted overgrowths formed 1759±18 Ma ago. Patchy zircons and CL-dark rims probably formed later but their age has not been established.

Grt-granulite Mk325

Six oval grains and grain fragments 40-130 μm in size were separated from this sample. Four of them exhibit blurred darker areas in CL, probably ghost cores, and broad homogeneous rims. The other two are patchy to homogeneous (Fig. 2d). The two largest grains were dated

by SHRIMP. In one of them, the core and the rim have been analyzed. These three spots show similar low U and Th contents, comparable to CL-bright homogeneous zircons from other samples, and yielded $^{207}Pb/^{206}Pb$ ages within the range 1545-1707 Ma. The Concordia age for two spots is 1656±31 Ma (Fig. 5d).

Grt-granulite Mk326.

This sample contains large (300-600 μm and larger) grains, sector-zoned and CL-dark, with coarse sectors, that were crushed into fragments, along with smaller (150-250 μm) polygonal grains having fir-tree sector-zoning in CL (Fig. 2c). Both large and small grains have CL-bright homogeneous rims and embayments. The textural difference between sector-zoned and fir-tree sector-zoned grains is not as obvious as the difference in compositions. Sector-zoned domains are characterized by high Th, U, Y and REE contents, Yb_N/Dy_N = 5.6-7.5 and negative Eu anomalies (Eu_N/Eu_N^* = 0.6). Fir-tree zircons have lower contents of these elements, Yb_N/Dy_N = 0.6 and a small positive Eu anomaly (Eu_N/Eu_N^* = 1.1). Bright homogeneous domains have moderate HREE concentrations and Yb_N/Dy_N = 2.1 (Fig. 3d). Most zircons form two groups with concordant ages of 1771±18 Ma and 1640±11 Ma (Fig. 5c). Two discordant spots within grain rims gave younger ages, down to 1562 Ma from $^{207}Pb/^{206}Pb$. The event that formed the homogeneous zircon should have caused re-setting of older generations. We suggest that the major age group (1640 Ma) reflects this event. In this case, the age of older generations is not determined.

Grt-granulite Mk523.

Over 30 grains 100-440 μm in size were separated from this sample. The grain shapes are irregular to polygonal or rounded. Larger grains have sector zoning in CL and darker rims that repeat the grain outlines and do not erase the sector-zoning. Smaller grains have blurred

sector-zoning that grades into a CL-bright homogeneous texture. Many of them have thick CL-dark rims (Fig. 2b). One homogeneous grain has an inclusion of plagioclase (An_{18}) which is similar to the groundmass plagioclase (An_{14}).

Sector-zoned zircons have low HREE contents with a negative HREE slope (Yb_N/Dy_N = 0.5) and a negative Eu anomaly (Eu_N/Eu_N^* = 0.7) (Fig. 3b). Homogeneous domains have almost half the Y and REE contents, but similar negative slopes of HREE and Eu anomalies in comparison to sector-zoned zircons. CL-dark rims are also similar to sector-zoned zircons but concentrations of REE and Y are higher by a factor of about 1.5. Th and U contents are similar in all three generation; Th/U is about 2 (Table 2).

Five of the largest grains were dated including cores and rims. Six of nine spots gave a Concordia age of 1740±16 Ma. One sector-zoned and one homogeneous domain show younger ages, down to 1.6 Ga; one CL-dark rim has an even younger age of ~1.3 Ga (Fig. 5e).

Two-pyroxene Grt-granulite Mk260

Eight zircon grains were found in this sample. One of them preserved a tiny piece of garnet attached to it with a similar composition to garnet from the matrix. The grains are rounded to oval, 70-150 μm in size. They have CL-dark polygonal sector-zoned cores and CL-bright sector-zoned to homogeneous rims (Fig. 2e). The cores are U-rich with Th/U = 0.03-0.25. They have weak positive HREE slopes and small negative Eu anomalies. Rims have shallower HREE slopes, negative Eu anomalies and lower U contents compared to the cores (Fig. 3c).

Five of the six spots have $^{207}Pb/^{206}Pb$ ages within 1905-1713 Ma. One spot is highly discordant with a $^{207}Pb/^{206}Pb$ age of 1116 Ma. Intercepts are at 948±360 and 1810±75 Ma (Fig. 5b). However, the oldest and youngest ages belong to CL-bright rims. The 1.81 Ga age is close to rim formation age, whereas cores were reset at this time and lost radiogenic Pb.

The youngest value (1116 Ma) is highly discordant, so the age of this superimposed event cannot be determined.

Grt-websterite Mk459

One zircon grain was found in thin-section between garnet, clinopyroxene and rutile grains. It has sector-zoning in CL and a darker rim that repeats its outline (Fig. 2f). This zircon has a negative HREE slope (Yb_N/Dy_N = 0.7) and a strong negative Eu anomaly (Eu_N/Eu_N^* = 0.34) (Fig. 4a). Three spots within the grain yielded $^{207}Pb/^{206}Pb$ ages from 1653 to 1700 Ma. Their concordia age is 1666±29 Ma (Fig. 5f).

Eclogite Mk284

A large zircon grain (500x300 μm) was found at a garnet-phlogopite boundary next to rutile, and small grains (50-150 μm) were found rimming large rutile grains. Zircon is bright and homogeneous in CL (Fig. 2j). It is characterized by very low Th and U contents (8-17 ppm), low REE contents, negative HREE slope (Yb_N/Dy_N = 0.8) and a lack of Eu anomaly (Fig. 4b). Seven spots within the large grain gave a range of $^{207}Pb/^{206}Pb$ ages from 1255 to 1651 Ma (Fig. 5i).

Phl-Grt-Opx rock Mk540

Two polygonal zircon grains 400x200 μm in size were found within a phlogopite grain. Zircon shows blurred sector-zoning and a narrow brighter rim in CL (Fig. 2i). The U content is 220 ppm and Th/U = 0.42 on average, but it decreases to 0.08 within CL-darker domains (Supplementary Data Electronic Appendices 6 and 7). CL-bright homogeneous rims have not been analyzed. Zircon shows a flat HREE pattern and a negative Eu anomaly (Fig. 4c). Six spots within the grain cores analyzed by LA-ICP-MS have $^{207}Pb/^{206}Pb$ ages of 1747-1723 Ma.

Their Concordia age is 1759±10 Ma (Fig. 5g). Three spots within low Th/U domains yielded $^{207}Pb/^{206}Pb$ ages from 1599 to 1707 Ma.

Grt-Phl-rock Mk172

One polygonal grain 400x100 μm in size was found within a phlogopite aggregate. It is almost homogeneous in CL with some very low contrast sectors (Fig. 2h) and has low Th and high U (480 ppm) concentrations and Th/U = 0.06. HREE contents are very low with a negative slope (Yb_N/Dy_N = 0.6) and a negative Eu anomaly (Eu_N/Eu_N^* = 0.6) (Fig. 4d). Two spots gave a Concordia age of 1659±19 Ma (Fig. 5h).

Phl-clinopyroxenite Mk536

Five polygonal grains 200-500 μm in size were found along a phlogopite-clinopyroxene boundary. They are characterized by sector-zoning, sometimes blurred (Fig. 2g). They have relatively low U contents (44 ppm on average) with Th/U = 1.1. HREE show a positive slope (Yb_N/Dy_N = 3.5) and a small negative Eu anomaly (Eu_N/Eu_N^* = 0.87) (Supplementary Data Electronic Appendix 6). Nine spots analyzed by LA-ICP-MS, mostly discordant, have $^{207}Pb/^{206}Pb$ ages from 1726 to 1661 Ma. Six of them gave a Concordia age of 1640±11 Ma (Fig. 5j).

Hf isotope composition of zircon and whole-rocks

Kola samples

Grt-granulite Mk 111. The five zircon generations all show similar Hf isotope compositions (Table 3). The oldest CL-dark sector zoned zircon has εHf(t) of -3.9. The other grains of this generation plot on a Pb-loss trajectory drawn for the oldest one on an εHf(t) vs $^{207}Pb/^{206}Pb$ age diagram (Supplementary Data Electronic Appendix 8). This confirms that young ages

obtained for three other CL-dark grains result from re-setting. Fir-tree zircons (the second metamorphic zircon generation), formed at 1918 Ma, have εHf(t) from -9.3 to -11.3 and are only slightly more radiogenic than CL-dark zircons; however, the difference does not exceed 2 ε units. CL-bright homogeneous grains yield εHf(t) from -11.0 to -11.7 at 1859 Ma. The overgrowths, patchy zircons and outer rims have εHf(t) from -15.3 to -13.1 at 1759 Ma. Together with homogeneous zircons, they plot close to the Pb-loss trajectories for fir-tree zircons (Fig. 6).

Grt-granulite Mk326. CL-dark sector-zoned first generation zircons formed at 1770 Ma or earlier have εHf(t) from -5.4 to -6.3 (Fig. 6, Table 3). Fir-tree sector-zoned second generation zircons with an age of 1640 Ma or older have εHf(t) from -10.2 to -9.2. Homogeneous zircon formed at 1640 Ma has a slightly more radiogenic Hf composition (εHf(t) = -8.4), but within 2ε units.

Grt-granulite Mk523. In all zircons, εHf(t) range from -7.9 to -5.9 at 1740 Ma (Fig. 6). No difference in Hf isotope composition between CL-dark rims and sector-zoned cores has been detected; however, this may be due to the size of sampling area which is comparable to the rim width and leads to mixed compositions.

Grt-websterite Mk459. A single spot has εHf(t) of -8.1 at 1666 Ma (Fig. 6, Table 3).

Eclogite Mk284. Two spots do not differ in their Hf isotopic composition: εHf(t) is -13.4 to -12.2 at 1651 Ma. The grain rim spot plots close to a Pb-loss trajectory for the core (Fig. 6, Table 3).

Grt-Phl-rock/glimmerite Mk172. Two spots within a single grain show the same εHf(t) of -15.5 (average) at 1659 Ma (Fig. 6, Table 3).

Arkhangelsk samples

Grt-granulite 60/473. Most zircon grains have dark oscillatory-zoned cores and CL-bright homogeneous rims. Sector-zoned domains surrounded by oscillatory shells are observed in some cores. Sector- and oscillatory-zoned zircons having a Concordia age of 2719±14 Ma show an average εHf(t) of -3.3 ± 1.4. CL-bright homogeneous rims have an age of 1805±26 Ma and an average εHf(t) of -22.8 ± 1.8 (Fig. 6, Table 3). A regression line for all data points coincides with a Pb-loss trajectory for spot 3.2 (with εHf(t) close to the average value for sector- and oscillatory-zoned zircons) on a plot εHf(t) vs $^{207}Pb/^{206}Pb$ age (Supplementary Data Electronic Appendix 8).

Grt-granulite P5/354. Three zircon generations occur in this sample: CL-dark sector zoned cores, CL-bright homogeneous shells and darker convoluted overgrowths on them. The cores vary in composition and have been divided into HREE-rich and HREE-poor groups (Koreshkova *et al*., 2014). Concordia ages of all zircons group at 1964±14 Ma and 1820±19 Ma. The younger value corresponds to the formation of overgrowths. The older one has been ascribed to a metamorphic event during which cores of different origin were equilibrated. The age of formation of homogeneous zircon is not well defined. The cores of both types have the same Hf isotopic composition (εHf(t) from -10.7 to -9.2 at 1964 Ma). The overgrowths and homogeneous zircons show similar εHf(t) at 1820 Ma, varying from -14.0 to -12.2. Data points for homogeneous zircons and the overgrowths lie close to Pb-loss trajectories for sector-zoned cores (Fig. 6).

Grt-granulite 77/690. Most zircon grains in this sample have CL-dark sector-zoned cores, CL-bright shells around them, and darker overgrowths with a convoluted texture. All of them yield the same age of 1836±15 Ma. Sector-zoned cores have εHf(t) from -24.2 to -22.4. Intermediate CL-bright shells have εHf(t) from -17.7 to -13.4. The scatter is due to some mixing, reflecting the sizes of zircon domains and sampling areas. The overgrowths yield εHf(t) from -10.3 to -7.6. These generations plot above each other on the εHf(t) vs $^{207}Pb/^{206}Pb$

age diagram (Fig. 6). Hence they have different sources and could not have been formed during the same event. We have suggested that cores and intermediate zones were completely reset during the formation of convoluted overgrowths (Koreshkova *et al*., 2014) and the Hf data confirm this interpretation.

Hf isotope composition of bulk-rocks

Hf bulk-rock analyses (Table 3 and Fig. 6) were made on five Grt-granulites previously studied by Kempton *et al*. (1995, 2001). Model T_{DM} ages are between 2.75 and 3.40 Ga. Present-day εHf values range from -44 to -19, correlating with their εNd values. However, sample N41-7 is displaced from the Terrestrial Array towards a lower εHf value.

Rb-Sr and Sm-Nd isotope composition of minerals and bulk-rocks

Garnets leached with H_2SO_4 show a decrease in Sm and Nd concentrations (up to 70% for Nd in sample 77/690) compared to unleached ones. They also show an increase in $^{147}Sm/^{144}Nd$ and $^{143}Nd/^{144}Nd$. Cpx-Grt(L) pairs from Mk111, Mk260 and 77/690 yield ages of 1536-1611 Ma, similar to those obtained by Kempton *et al*. (2001). The slope of the Grt-Cpx tie-line in eclogite Mk284 corresponds to an age of 1735 Ma (Supplementary Data Electronic Appendix 9). No leaching experiments were undertaken for this sample because of the small amount of material. The point for pargasite plots close to the line Grt-Cpx, whereas phlogopite lies significantly above it. In this sample, the minerals are not in Nd isotopic equilibrium. Secondary mineralization along cracks in phlogopite can also contribute to the apparent disequilibrium. However, in the Rb-Sr system, the minerals show a better approximation to an isochron relationship. The slope of the Cpx-Prg-Grt-Phl line corresponds to an age of 1304±63 Ma.

DISCUSSION

Mineral compositions and zoning

Most lower crustal xenoliths from both Kola and Arkhangelsk exhibit similar major element zoning patterns in garnet and pyroxene. Garnets show some increase in CaO content and decrease in Mg# from grain cores to rims. The profiles are convex-upward for Mg# and trough-like for Ca, with a flat central zone (Fig. 7a, b). Some samples (Mk260, Mk459, Mk540, 77/690) do not display any noticeable change of CaO content. Pyroxenes show increasing Mg# and decreasing Al_2O_3 contents from core to rim. In Grt-granulites, zoning is stronger at garnet-pyroxene boundaries and much less developed at boundaries with plagioclase. We suggest that zoning in MgO and FeO in garnet and pyroxene and CaO in garnet was due to diffusional exchange during final cooling and was superimposed onto more or less homogeneous grains. Al in pyroxenes could preserve growth zoning, at least partially, because of its lower diffusion rate compared to Fe and Mg.

In contrast, garnet and clinopyroxene show significant zoning in REE and HFSE. Partitioning of these elements is strongly pressure- and temperature-dependent. Y and HREE contents in garnet decrease with increasing temperature (Rubatto & Hermann, 2007). Sun & Liang (2015) have shown that $D^{Grt/Cpx}$ for REE decreases by up to two orders of magnitude as temperature decreases from 1300 to 700 °C, whereas it increases by about one order of magnitude as pressure decreases from 14 to 2 GPa. $D^{Grt/Cpx}$ for Zr also depends significantly on pressure and temperature. Nehring *et al*. (2010) reported values of around 0.2 for granulites from Central Finland for which peak metamorphic conditions are 800-950 ^{o}C and 0.9-1.1 GPa; Zack *et al*. (1997) reported a value of 0.86 for Grt-pyroxenite xenoliths equilibrated at 920 ^{o}C and an assumed pressure of 1.5 GPa; Rubatto & Hermann (2003) suggested a value of 2.9 for an eclogite equilibrated at 600-620 ^{o}C and 2 GPa; Klemme *et al*. (2002) experimentally determined a value of 4.2 in synthetic eclogite at 1400^{o}C and 3 GPa.

REE diffusion rates in garnet and pyroxene are slower than those of divalent cations (Van Orman *et al*., 2001, 2002). Y and HREE in garnets have similar diffusivities (Carlson, 2012; Bloch et al., 2015), whereas those for Hf are significantly lower than for REE (Bloch *et al*., 2015).

Garnets from the Kola and Arkhangelsk lower crustal xenoliths differ in HREE and Y zoning patterns. In the Arkhangelsk samples, garnets show a strong decrease in HREE and Y, comparable in magnitude to the zoning in Zr and Hf (Fig. 7e). We have previously suggested (Koreshkova *et al*., 2014) (and our opinion remains the same) that the garnets from the Arkhangelsk Grt-granulites retained their growth zoning, due to Rayleigh distillation. These samples contain abundant zircon. Its formation prior to garnet determined the low Zr and Hf in the latter, but the concentrations decrease to one third from cores to rims.

Most garnets and clinopyroxenes from the Kola lower crustal xenoliths only exhibit significant zoning in Zr and Hf. The contents of Y and HREE in garnets mostly decrease by ca 10% within an outer zone 100-500 μm wide (Fig. 7c-d). Patterns like these can be a result of either growth at relatively high temperature (combined effect of initial low Y and HREE contents, Rayleigh distillation and diffusional homogenization) or re-equilibration at the onset of high temperature and slow cooling. The Zr contents in garnets decrease by half towards grain rims. We have observed a dependence of zoning magnitude on neighboring phases. In Grt-granulites, the difference in Zr content between the cores and rims of garnet and clinopyroxene grains is smaller when they are in contact with each other and stronger in contact with plagioclase. This is more consistent with re-equilibration. Further evidence for later diffusional homogenization is the composition of zircons from samples Mk326 (fir-tree) and Mk523 that should have co-existed with garnet with a lower HREE content (Yb_N/Dy_N < 0.6) than those actually present in these samples (Yb_N/Dy_N = 0.8-1.0). We suggest that the garnets were re-equilibrated at relatively high temperature, so that they have lost their initial

growth zoning in Y and HREE, but partially preserved zoning in Zr and Hf because of the difference in the diffusivities of REE and Hf (Bloch *et al*., 2015) and the expected similar behavior of Zr and Hf. It would take about 30 Myr to eliminate zoning in Lu, but not in Hf, in a garnet grain with a radius of 850 μm at 900 ^{o}C, which are the parameters corresponding to Grt-granulite Mk523 (using an expression $t \approx 1.11 * a^2/D$, where t is time in seconds, a – grain radius in cm, D – diffusion coefficient; diffusivities of Lu and Hf from Bloch *et al.* (2015a,b)).

As a first approximation, we can take the Zr contents of garnets and clinopyroxenes unaffected by later re-equilibration. In our samples, $D^{Grt/Cpx}$ of Zr varies mostly within the range 0.1-0.3, being higher in grain cores and lower in rims. The Arkhangelsk samples show slightly lower values (0.1-0.2) than those from Kola (0.1-0.5). The highest values of 0.4-0.5 are from Grt-websterite Mk459 and Phl-eclogite Mk284 (Fig. 8a). This distribution is consistent with P-T estimates for xenoliths from Kola and Arkhangelsk, which are similar to those for granulites from Finland (Nehring *et al*., 2010), but with a higher pressure for some Kola xenoliths. Covariations of Zr contents in garnet, clinopyroxene and rutile suggest their equilibrium (Fig. 8b-c), except for rutile from Mk284. In this sample, rutile with low Zr content is rimmed by small zircon grains that could have been formed later than the closure of diffusional exchange with garnet and clinopyroxene. In summary, zoning in Zr, Hf, Y, HREE, Al, Ca and Mg# in garnets and clinopyroxenes reflects different stages of their existence: growth, homogenization, and diffusional exchange during final cooling.

Growth under increasing temperature can explain the decrease of Y and HREE from cores to rims in garnets, but it should be accompanied by increasing Ti, Zr and Hf contents. This is probably the case for eclogite Mk284 where intermediate zones of garnet grains show strong increases in the contents of these elements (Fig. 7f). The size of clinopyroxene grains is smaller than that of garnets. From $D_{Zr}^{Grt/Cpx}$, it is probable that Cpx cores co-existed with

garnet intermediate zones (Fig. 8a). The source of Ti, Zr and Hf was dissolution of zircon and rutile.

To consider zircon-garnet equilibrium in Grt-granulites, we have used experimentally determined $D^{zrn/grt}$ for REE and Y (Rubatto & Hermann, 2007). Grt-granulites are suggested to have experienced partial melting; thus zircon and garnet could have been in equilibrium with a silica-rich melt. Only the youngest zircon generations from samples Mk111 (overgrowths) and Mk326 (homogeneous rims) match the calculated composition of zircon in equilibrium with garnet present in the rock (Table 2, Fig. 3). Other zircon generations from these samples and zircons from samples Mk260 and Mk523 could have equilibrated with garnet, but of a different composition, having either higher or lower HREE contents.

Pargasite should have Zr and Hf contents equal to those of clinopyroxene (Nehring *et al*., 2010) but, in our samples, it has only half of the concentrations and contains numerous inclusions of rutile formed by exsolution. In the Kola samples, rutile often shows zircon exsolution. Consequently, Zr could be released from rutile and pargasite during a retrograde metamorphic event or slow cooling.

Phlogopites in Mk540 and Mk172 have higher Nb, Ta and REE contents than those from Grt-granulite Mk326 and eclogite Mk284. In Mk540 and Mk172, phlogopites have also much higher Zr and Hf contents than in Mk326, Mk284 and clinopyroxenite Mk536. This suggests that these phlogopites were not equilibrated with rutile and zircon; hence they are a later addition to the rocks.

Hf isotopes and sources and mechanisms of zircon formation

Magmatic zircons in Grt-granulite 60/473 show two generations: sector-zoned cores and oscillatory overgrowths with $^{207}Pb/^{206}Pb$ ages from 1948 to 2746 Ma (Koreshkova *et al*., 2014). Hf isotopes confirm that the younger ages are due to Pb-loss and partial re-setting

during a 1.8 Ga metamorphic event. The difference in age between the two generations has not been resolved. Sector- and oscillatory-zoned zircons do not differ in their Hf isotopic composition. These two generations hence could have crystallized from a similar source and close in time. Their REE contents do not contradict crystallization from a melt with a composition corresponding to this sample (Koreshkova *et al.*, 2014). Their εHf values (-4 to -1) suggest formation from an enriched source or re-setting of older zircons which originated from melts of depleted mantle. The parental melt had an Hf isotopic composition similar to the protoliths of the Kola Grt-granulites (Fig. 6).

Recrystallization and exsolution

In Grt-granulite 60/473, CL-bright homogeneous rims have the least radiogenic Hf among the samples (εHf(t)=-24 to -23). Their Hf isotopic composition does not differ from that of magmatic cores (Fig. 6). Previously, we suggested that homogeneous zircon was formed by recrystallization of earlier magmatic zircon (Koreshkova *et al*., 2014). Recrystallization proceeds by grain-boundary and defect migration, as discussed by Hoskin & Schaltegger (2003). In this process, U, Th, Pb, REE and Y are variously removed from the zircon lattice, but not Hf, and no growth of new zircon occurs; thus zircon yields the U-Pb age of metamorphism and the Hf isotopic composition of its precursor. In sample 60/473, Hf data are consistent with the rims being formed by recrystallization of ancient magmatic zircons.

Homogeneous, CL-bright, Th- and U-poor zircons were also formed as rims or whole grains in samples Mk523, Mk326, Mk284, Mk111 and P5/354. In each case, the zircons do not differ from previous zircon generations in terms of Hf isotopes (except for Mk284 where it is a single generation). In Mk523 and Mk326, they are the latest generations formed after metamorphic zircons having the most radiogenic Hf with εHf(t) = -8 to -6. In Mk111 and P5/354, homogeneous zircons were formed after metamorphic zircons older than in Mk523

and Mk326, and show intermediate εHf(t) values (-13 to -11) at 1.86 Ga (Fig. 6). We suggest that these zircons are also recrystallized. The Hf isotopic composition of zircons from P5/354 is consistent with our previous conclusion that dark sector-zoned cores are metamorphic and bright, homogeneous zircon domains were formed by recrystallization of the cores. Our new data also demonstrate that the CL-bright sector-zoning is a ghost texture, due to incomplete recrystallization. In these zircons, REE and Y contents vary from sample to sample. They are mostly lower than in their precursor zircons, but Grt-granulite Mk326 provides an example of higher concentrations of HREE and Y in homogeneous zircon in comparison to the previous zircon generation. We infer that the REE contents in recrystallized zircons, as in subsolidusly-grown ones, could depend on the conditions of equilibration.

Structureless BSE/CL rims, which do not differ in their Hf isotopic composition from cores, have been reported by Zheng *et al.* (2004) for zircons from lower crustal granulite xenoliths from China. These authors concluded that the rims were formed by recrystallization of older zircons based on Hf data. Vavra *et al*. (1999) and Harley & Kelly (2007) have related the formation of CL-bright homogeneous rims and domains in zircons to interaction with a fluid. We have no evidence for the presence of fluid, such as porosity or corroded surfaces, but after zircon formation the rocks were still under granulite-facies conditions and fluid interaction features (if any) may have been lost. However, more important is that these recrystallized CL-bright homogeneous zircons were formed from their precursors without addition of new material, i.e., no zircon-producing reaction and, probably, no major change of mineral association occurred.

CL-dark outer rims of the last zircon generations from samples Mk111, Mk523 and Mk459 developed on different zircon types and show ghost textures. They could also have been formed by recrystallization. The rims exhibit an enrichment in REE and Th, as seen in rims developed on CL-bright homogeneous zircon from Mk111. Recrystallization proceeds by

defect migration (Hoskin & Schaltegger, 2003) that may help zircon adjust its composition to changing ambient conditions. Reddy *et al.* (2006) documented enhanced diffusion of REE during dislocation creep in zircon. As a suggestion, variable removal or enrichment in Th, U and REE in recrystallized zircons could depend on conditions of equilibration and changes in matrix composition.

In zircon from eclogite Mk284, the Hf isotopic composition (εHf(t) = -13 at 1.65 Ga) is similar to that of zircons from the granulites, which implies that it is not a later addition from a mantle source. Zoning of garnet from Mk284 records a high-temperature event (Fig. 7) when zircon could have been dissolved. From the distribution of Zr between garnet, clinopyroxene and rutile, it follows that zircon could have been formed by exsolution from rutile, later than the formation of garnet rims (Fig. 8). This zircon could have equilibrated with garnet (Fig. 4b). Therefore, this zircon might indicate a retrograde metamorphic event or slow cooling. In this sample, we cannot distinguish between the different possibilities of zircon formation such as subsolidus growth due to a reaction involving rock-forming minerals, exsolution from rutile or recrystallization. The Hf isotope composition does not contradict either possibility.

Subsolidus zircon growth

Sector-zoned and convoluted zircons formed by subsolidus growth have εHf(t) varying from -24 to -4 (Fig. 6). First zircon generations from samples P5/354 and Mk111 (CL-dark sector-zoned zircons) are suggested to have co-existed with garnet which had low HREE contents (see section "*Mineral compositions and zoning*"). These are the oldest metamorphic zircons in the sample suite. In Mk111, εHf(t) was -4 at 2.25 Ga (Supplementary Data Electronic Appendix 8). In P5/354, εHf(t) was -9 to -11 at 1.96 Ga. The sources of these zircons had Hf isotopic compositions similar to bulk-rock samples from Kola.

The second zircon generation from Mk111 (fir-tree sector-zoned zircon) differs significantly from the first one in its REE composition, but is similar in Hf isotopic composition (Supplementary Data Electronic Appendix 8). The youngest zircon generations from samples P5/354 and Mk111 (overgrowths with convoluted texture) also have Hf compositions that do not differ from older generations (within 2 εHf units) (Fig. 6). These zircons grew in equilibrium with garnet; however, their precursors were also formed in the presence of garnet but of a different composition, as follows from previous discussions in the section "*Mineral compositions and zoning*". Similarly, in Grt-granulite Mk326, the second generation (fir-tree sector-zoned zircon), which indicates the appearance of garnet in this rock, has the same Hf isotopic composition as older zircon which formed in the absence of garnet. The source material for these zircons should have very low Lu/Hf, such as found in zircon and rutile or in minerals equilibrated with garnet, and thus have low Lu, such as pargasite and diopside. These minerals should retain the Hf isotopic composition from the earlier metamorphic stage when they crystallized to provide non-radiogenic Hf for a newly-formed zircon. Earlier-formed garnet could not have been involved in the zircon-producing reaction; otherwise it would have supplied radiogenic Hf. The possibility of radiogenic Hf being supplied by garnet has been demonstrated by Sláma *et al*. (2007) for amphibole, orthopyroxene and, possibly, zircon formed during a garnet decompression reaction. Dissolution of older zircon and reprecipitation, with the formation of a new zircon generation with the same Hf isotopic composition has been proposed for zircons from granulite-facies metapelites of the Ivrea-Verbano zone (Ewing *et al*., 2014). Rutile often shows zircon exsolution in lower crustal xenoliths (e.g., Schmitz & Bowring, 2003). Rutile can retain its Hf isotopic composition from the time of its formation (Ewing *et al*., 2014).

In most samples in the suite, clinopyroxene is one of major Zr- and Hf-bearing phases (it contains 40-60 wt% of the whole-rock budget of Zr and Hf, except for Grt-granulite P5/354).

In P5/354, the most plausible sources of Zr for the overgrowths are rutile and pre-existing zircon, because this metasedimentary rock probably was never clinopyroxene- or amphibole-rich. These overgrowths have been suggested to date a partial melting event with garnet in the residue (Koreshkova *et al*., 2014). We suggest the same source for the second generation (fir-tree sector-zoned zircon) from Mk326 because there was no earlier-formed garnet. For the second zircon generation from Mk111 (fir-tree sector-zoned zircon), the source could be clinopyroxene, pargasite, rutile or previous zircon, provided that garnet formed earlier was not involved in the zircon-producing reactions. The fourth zircon generation in Mk111 (convoluted overgrowths) could have no phases formed at previous metamorphic stages as the source of Zr, except for zircon itself. This is illustrated schematically on $^{176}Hf/^{177}Hf$ vs time plot for Mk111 (Fig. 9a).

In zircon from Grt-Phl-rock Mk172, the Hf isotopic composition (εHf(t) = -15 at 1.65 Ga) is similar to that of zircons from the granulites which implies it is not a later addition from a mantle source. This zircon might be formed by subsolidus growth in the presence of garnet under high-pressure-high-temperature conditions.

Most radiogenic (εHf(t) = -10 to -5) zircons are from samples Mk523, Mk459, Mk326 and the latest of the three generations from sample 77/690 (Fig. 6). In the latter case, the overgrowths probably formed at the beginning of garnet growth via garnet-forming reactions such as Hbl + Pl + Qtz = Grt + Cpx + liquid or vapour (Koreshkova *et al*., 2014). In Mk326, the first generation of sector-zoned zircon should also have been formed before garnet appeared in the rock, according to its high HREE contents and Yb_N/Gd_N ratio. Zircons from samples Mk523 and Mk459 grew in the presence of garnet, as follows from their low HREE. However, garnet in equilibrium with zircon in Mk523 should have lower HREE contents and Yb_N/Gd_N than the measured values (see above, Table 2). This can be explained by a change of garnet composition from low HREE (formed at high temperature or strongly zoned as in

60/473) towards the observed composition. The partition coefficients might not apply to Grt-pyroxenite Mk459, but we think the situation is similar. Hence in samples Mk523 and Mk459, garnet was either formed together with zircon or was present in earlier mineral associations, but it must have been involved in zircon-producing reactions to supply radiogenic Hf. In other words, it did not hold the radiogenic Hf that it extracted from the source of the zircon. Probably, garnet and zircon grew together, and zircon equilibrated garnet which had low HREE. Later, during a high-temperature event or slow cooling, the garnet re-equilibrated and attained its present composition. In summary, for zircons with radiogenic Hf isotope compositions, the source of the zircon could be the rock as a whole, in which the Hf isotopic composition evolved with time.

We suggest a similar origin for CL-bright intermediate zones from Grt-granulite 77/690 that represent a subsolidus zircon generation younger than the cores and older than the overgrowths, but reset during the formation of the overgrowths (Fig. 6). Zircon cores from 77/690 differ from all other sub-solidus zircons in having a non-radiogenic Hf isotopic composition similar to the magmatic and recrystallized zircons from Grt-granulite 60/473 (Fig. 6). The cores were reset during the granulite-facies event 1836 Ma (Fig. 9b). They could have originated by dissolution and re-precipitation of Archaean magmatic zircons, otherwise they represent ancient magmatic zircons with modified textures.

Zircon ages and their significance

The age data for the metamorphic zircons can be divided into five groups: >1.91 Ga, 1.81-1.86 Ga, 1.74-1.77 Ga, 1.64-1.67 Ga and <1.6 Ga. The relationship of the zircons to their present-day mineral associations is summarized in Fig. 10.

First Group

The first group comprises zircon cores from Grt-granulites Mk111, Mk260 and P5/354. The oldest zircon in the group is CL-dark sector-zoned zircon from Mk111 that equilibrated with garnet at high temperature and hence provides evidence of a >2.2 Ga, pre-Lapland-Kola, metamorphic event.

Other zircon ages from this group correlate with metamorphic events superimposed onto the rocks of the Belomorian Belt during Lapland granulite belt formation: arc magmatism and metamorphism starting from 1.98 Ga, collision of island arcs with the continent at ~1.95-1.93 Ga and the main collision of juvenile rock complexes and the Karelian craton at 1.93-1.90 Ga (Mintz *et al*., 1996; Daly *et al*., 2001; Daly *et al*., 2006; Glebovitsky *et al*., 2009; Tuisku *et al*., 2012). In P5/354, the oldest age–group (1964±14 Ma) comprises zircons having significantly different compositions: (low HREE + low Th/U) vs (high HREE + moderate Th/U). These zircons were formed in the presence and in the absence of garnet, respectively. This means that either one of the compositional varieties was reset and the other one was formed during the metamorphic event, or both of them were reset and hence they are inherited and came from pre-existing metamorphic rocks. However, all these zircons have the same Hf isotopic composition. We suggest that one of these varieties was formed by dissolution and reprecipitation of the other. The composition of the next zircon generation points to the co-existence with earlier-formed garnet. Thus, this age group dates a granulite-facies event when garnet and low-HREE-zircon were formed.

The second zircon generation (fir-tree) in Mk111 was formed at 1918 Ma. Orthopyroxene inclusions and a strong negative Eu anomaly in this zircon indicate the presence of plagioclase and orthopyroxene in the mineral association at this time. Garnet could have been present, as follows from the moderate HREE slope in this zircon. If garnet were present, it would have differed in composition from those which co-existed with previous sector-zoned zircon and the next generation, and the garnet-zircon pair could have been formed under much

lower temperature conditions than their precursors. This zircon dates the formation of the Opx-Pl±Grt-bearing association (distinct from the pre-existing one).

Zircon cores from Mk260 are suggested to be no younger than 1905 Ma. Their small Eu anomalies indicate that plagioclase was not abundant at this time. The mineral association was different from the present one because of the significant difference in composition between this and the next zircon generation. The association probably corresponded to a Grt-websterite, taking into account the bulk-rock composition.

Second Group

In the second group, recrystallized zircons from Grt-granulites Mk111 (1859±13 Ma) and 60/473 (1805±26 Ma) and overgrowths from Mk260 (1810±60 Ma), P5/354 (1820±19 Ma) and 77/690 (1836±15 Ma) are present. Their ages correspond to the youngest collisional amphibolite-facies event in the upper crustal rocks (Bibikova *et al*., 2001, 2004). Recrystallized zircons date the onset of high temperatures that triggered diffusional exchange of the zircons with their environment. The zircons differ in REE composition from sample to sample, which points to different formation conditions. In 60/473, the zircon could be in equilibrium with garnet at about 800 ^{o}C (Koreshkova *et al*., 2014), whereas in Mk326, the temperature could be about 900 ^{o}C (Fig. 3d).

The overgrowths in P5/354 were in equilibrium with garnet cores at 950-1000 ^{o}C (Koreshkova *et al*., 2014) and were formed by dissolution and precipitation of older zircons according to their Hf isotope composition. Partial melting is suggested from the plausible reaction of biotite and quartz, with garnet in the residue. In this case, the overgrowths could have crystallized from a small-volume partial melt. The overgrowths in Mk260 were formed at a similar temperature in the presence of garnet. In 77/690, the overgrowths were formed in the course of the garnet-producing reaction (Koreshkova *et al*., 2014) involving all phases. In

general, the overgrowths in these samples date a major change in mineral associations including partial melting.

Third Group

The third group includes the overgrowths from Mk111 (1759±18 Ma) and sector-zoned zircons from Mk523 (1740±16 Ma) and Mk540 (1759±10 Ma). In Mk111, the overgrowths were formed at 950 ^{o}C according to our calculations (Fig. 3a, Table 2), during the formation of the present mineral association. This zircon could have formed from clinopyroxene, pargasite or rutile, composing the association of the previous metamorphic stage, and, or, by dissolution-reprecipitation of previously existing zircon. Small Eu anomalies in Zrn and Grt can reflect a decrease in Pl abundance, possibly during a Grt-forming reaction (such as Cpx+Pl→Grt+Qtz). Zircon from Mk523 grew in the presence of garnet, with the whole-rock as its source. In Mk540, zircon and garnet have similar HREE slopes and Eu anomalies (Fig. 4c) and could have been formed together. We suggest that the zircons from this group date a granulite facies event in the lower crust which coincided with pegmatite formation in the regional upper crust (Bibikova *et al*., 2001, 2004) and post-collisional granite emplacement in the northwestern part of the Lapland belt (Daly *et al*., 2006).

Fo*urth Group*

The fourth group contains recrystallized zircons from Grt-granulites Mk326 (1640±11 Ma) and Mk325 (1659±31 Ma) and sector-zoned zircons from samples Mk459 (1666±29 Ma), Mk172 (1659±19 Ma) and Mk536 (1640±11 Ma). In Grt-granulite Mk326, homogeneous zircon was formed by recrystallization and equilibrated with garnet at 900 ^{o}C and hence dates the onset of high temperature for the mineral association. We suggest that the same is true for Mk325. Zircon from Grt-websterite Mk459 possibly formed during the garnet-producing

reaction and in the presence of plagioclase, as follows from its negative Eu anomaly. This explains its radiogenic Hf isotope composition. However, a later change of garnet composition suggests that the zircon age may reflect partial re-setting. In clinopyroxenite Mk536, zircon has a texture and composition similar to magmatic zircon and plausibly dates the formation of this rock. We suggest that two samples from this group (Mk326 and Mk536) contain zircons that have been formed in this time interval. This event of zircon formation and re-setting significantly postdates Lapland-Kola events in the regional upper crust and may be related to the onset of Mesoproterozoic rifting in the East European plate (Bogdanova *et al*., 2008).

Fifth Group

The fifth group comprises single grains from samples Mk111, Mk523, Mk540 and CL-bright homogeneous zircon from eclogite Mk284. Their $^{207}Pb/^{206}Pb$ ages vary from 1599 to 1255 Ma. Most of them are reset zircons of older generations. The youngest values belong to the CL-dark outer rim from Grt-granulite Mk523 (1348 Ma) and peripheral area of the large grain from eclogite Mk284 (1255 Ma). U-Pb zircon dating and Rb-Sr data for Mk284 suggest that its mineral association was formed not later than 1.3 Ga. We suggest that around this time an event reset some individual zircon grains and activated diffusion which led to the formation of CL-darker rims in samples Mk111 and Mk523. However, this assumed event is younger than the Sm-Nd ages of Grt-Cpx pairs from our samples (Supplementary Data Electronic Appendix 9).

We suggest that Sm-Nd ages of Grt-Cpx pairs correspond to the time when the closure temperature of Sm and Nd isotope exchange was achieved in these minerals at 1.54-1.61 Ga, within both the Arkhangelsk and Kola parts of the Belomorian Mobile Belt. If we assume that the peak temperature during the last granulite-facies event at 1640 Ma (U-Pb zircon age) was

ca 900 ^{o}C, and, at 1560 Ma (Sm-Nd age of Grt-Cpx pair from Mk111), the temperature was around 600 ^{o}C which is close to an average value for grain rims (Table 1), then the cooling rate was about 4^{o}/Myr. The closure temperature (Dodson, 1973) of Sm diffusion in a Grt grain with a radius of 1-3 mm, using diffusivities from Tirone *et al*. (2005), would be 570-630 ^{o}C.

Zircons from phlogopite-rich rocks do not directly date the timing of phlogopite appearance. In Mk540, zircon predates its introduction. In Mk284, zircon postdates phlogopite, whereas zircon from Mk172, which is similar to Mk540, could have been reset. Probably only clinopyroxenite Mk536 contains zircon formed during the crystallization of this phlogopite-bearing rock. If there was a single event of phlogopite introduction, we can take its age as ca 1.64 Ga. However, there might not have been a single event, but several events. Kempton *et al*. (2001) argued, based on Ar-Ar dating of phlogopite, that it was formed at about 2.1 Ga.

Peltonen *et al*. (2006) obtained both Archean and Proterozoic ages in zircons from granulite xenoliths from eastern Finland. They argued that the lower crust of the Karelian craton is composed partially of Archean rocks reworked during the Svecofennian orogeny. However, they also found “post-orogenic” zircons with ages of around 1.7 Ga for which no events are known in the upper crust. On the northeastern boundary of the Karelian craton, later pegmatite intrusions occurred at 1.75 Ga; the latest event was the intrusion of the ultrapotassic minettes of Porja Guba at 1720±8 Ma (Nikitina *et al*., 1999). We suggest that deep-seated rocks were affected by the Mesoproterozoic rifting more significantly than the upper crustal rocks (possibly by mantle-derived fluids).

The present-day garnet-granulite association was formed at 1.83 Ga in the Arkhangelsk xenoliths and 1.74-1.76 Ga ago in most Kola xenoliths. Nevertheless, samples Mk111 and Mk260 have zircons formed earlier, in granulite-facies conditions. We conclude that, by the

end of the Lapland-Kola orogeny, the rocks were already assembled together in the lower crust and metamorphosed under granulite facies conditions.

The protoliths of most xenoliths could be Archean, but this does not mean they were already present in the lower crust. These Archean zircons have steep HREE slopes and could have crystallized from magmas at low pressure. However, preservation of pre-Lapland-Kola granulite facies zircon in Mk111 suggests that some samples represent an older lower crust. The composition of the first zircon generation in Mk326 resembles magmatic zircon. If it is magmatic, the protolith of this xenolith is not older than 2.41 Ga and is the youngest addition to the 2.7-3.4 Ga suite.

CONCLUSIONS

Metamorphic zircons from lower crustal mafic granulite and pyroxenite xenoliths from NW Russia have highly variable εHf(t) values from -25 to -4. The least radiogenic are zircons which formed by recrystallization of primary magmatic Archean zircons (present in grain cores) and which retained their Hf isotopic composition. The source of those zircons with the most radiogenic Hf (εHf(t) from -10 to -4) was the host-rock as a whole. These zircons grew before garnet or were contemporaneous with its formation. In some samples, garnet could have been present in earlier mineral associations but it must have been involved in zircon-producing reactions to supply radiogenic Hf. Zircons with less radiogenic Hf compositions (εHf(t) from -15 to -9) were formed by recrystallization of pre-existing metamorphic zircons or by subsolidus growth in the presence of garnet, or by exsolution from rutile. They inherited their Hf isotopic composition from clinopyroxene, pargasite, rutile and earlier-formed zircon equilibrated with garnet. Subsolidus zircons grew in response to a major change in mineral association, i.e., garnet- and zircon-producing reactions including small-volume partial

melting. CL-bright homogeneous recrystallized zircons date the onset of high temperatures that triggered diffusional exchange of zircon with its environment.

Most zircons only preserved a record of the latest metamorphic events. The exceptions are Grt-granulites 60/473 from Arkhangelsk and 16/89 from Kola (Downes *et al*., 2002) that retained Archean magmatic zircons. We suggest that Arkhangelsk zircons are derived from the protolith, rather than being inherited. Their εHf values (-4 to -1 at 2.72-2.74 Ga) suggest formation from an enriched source or re-setting of older zircons which originated from melts from the depleted mantle. The parental melt had a Hf isotopic composition similar to the protoliths of Grt-granulites from Kola.

Age data for metamorphic zircons can be divided into five groups: >1.91 Ga, 1.81-1.86 Ga, 1.74-1.77 Ga, 1.64-1.67 Ga and <1.6 Ga. The oldest is CL-dark sector-zoned zircon from Grt-granulite Mk111 that was equilibrated with garnet at high temperature and hence is evidence of a >2.2 Ga, pre-Lapland-Kola, metamorphic event. The age ranges of 1.92-1.94, 1.81-1.86 and 1.74-1.77 Ga correlate with Lapland-Kola metamorphic events in the regional upper crust. These zircons date granulite facies metamorphic events in the lower crust. Zircon formation and re-setting at 1.64-1.67 Ga significantly postdates the Lapland-Kola events and may be related to the onset of rifting in the Late Paleoproterozoic. Cooling began after this, as seen from Sm-Nd data. The youngest ages (1.6-1.3 Ga) correspond to an event or events that affected only few grains in some samples. A possible explanation is interaction with a localized fluid.

The present-day garnet-granulite association was formed at 1.83 Ga in the Arkhangelsk xenoliths and at 1.74-1.76 Ga in most Kola xenoliths. Nevertheless, some samples (Mk111, Mk260 and P5/354) have zircons formed earlier in a granulite facies environment. We conclude that by the end of the Lapland-Kola orogeny the rocks were already assembled together in the lower crust and metamorphosed under granulite facies conditions. However,

no addition of juvenile material younger than 2.4 Ga has been detected. Preservation of pre-Lapland-Kola granulite facies zircon in Mk111 suggests that some samples represent an older lower crust. Granulites, pyroxenites and Phl-rich rocks have had a common metamorphic history since at least ca 1.75 Ga. At about 1.64 Ga metasomatic introduction of phlogopite took place; however, there could have been several earlier phlogopite-forming events.

ACKNOWLEDGEMENTS

We thank Dr Andy Carter, Dr Martin Rittner and Dr Andy Beard (Birkbeck) for technical help with microprobe and laser probe analyses, and Dr Sergey Presniakov (VSEGEI) who analyzed zircons from sample Mk260. We thank the reviewers Dr Svetlana Bogdanova and Dr Elias Bloch for their constructive and thorough reviews.

FUNDING

We gratefully acknowledge Russian Federal budget funding, Scientific Research Work № 3.42.1412.2015.

REFERENCES

Beard, A.D., Downes, H., Vetrin, V., Kempton P.D. & Maluski, H. (1996). Petrogenesis of Devonian lamprophyre and carbonatite minor intrusions, Kandalaksha Gulf (Kola Peninsula, Russia). *Lithos* **39**, 93-119.

Beard, A.D., Downes, H., Hegner, E. & Sablukov, S.M. (2000). Geochemistry and mineralogy of kimberlites from the Arkhangelsk Region, NW Russia: evidence for transitional kimberlite magma types. *Lithos* **51**, 47-73.

Bibikova, E., Skiöld, T., Bogdanova, S., Gorbatschev, R. & Slabunov, A. (2001). Titanite-rutile thermochronometry across the boundary between the Archaean Craton in Karelia and the Belomorian Mobile Belt, eastern Baltic Shield. *Precambrian Research* **105**, 315–330.

Bibikova, E.V., Bogdanova, S.V., Glebovitsky, V.A., Claesson, S. & Skiöld, T. (2004). Evolution of the Belomorian Belt: NORDSIM UPb Zircon Dating of the Chupa Paragneisses, Magmatism, and Metamorphic Stages. *Petrology* **12**, 195-210.

Bloch, E., Ganguly, J., Hervig, R. & Cheng, W. (2015a). ^{176}Lu–^{176}Hf geochronology of garnet I: experimental determination of the diffusion kinetics of Lu^{3+} and Hf^{4+} in garnet, closure temperatures and geochronological implications. *Contributions to Mineralogy and Petrology* **169**, 12.

Bloch, E., Ganguly, J., Hervig, R. & Cheng, W. (2015a). ^{176}Lu–^{176}Hf geochronology of garnet I: experimental determination of the diffusion kinetics of Lu^{3+} and Hf^{4+} in garnet, closure temperatures and geochronological implications. *Contributions to Mineralogy and Petrology* **169**, 12.

Bogdanova, S.V., Bingen, B., Gorbatschev, R., Kheraskova, T.N., Kozlov, V.I., Puchkov, V.N. & Volozh, Yu.A. (2008). The East European Craton (Baltica) before and during the assembly of Rodinia. *Precambrian Research* **160**, 23-45.

Carlson, W.D. (2012). Rates and mechanisms of Y, REE, and Cr diffusion in garnet. *American Mineralogist* **97**, 1598–1618

Daly, J.S., Balagansky, V.V., Timmerman, M.J., Whitehouse, M.J., de Jong, K., Guise, P., Bogdanova, S., Gorbatschev, R. & Bridgwater, D. (2001). Ion microprobe U-Pb zircon geochronology and isotopic evidence for a trans-crustal suture in the Lapland–Kola Orogen, northern Fennoscandian Shield. *Precambrian Research* **105**, 289-314.

Daly, J.S., Balagansky, V.V., Timmerman, M.J. & Whitehouse, M.J. (2006). The Lapland-Kola orogen: Palaeoproterozoic collision and accretion of the northern Fennoscandian

lithosphere. In: Gee, D.G. & Stephenson, R.A. (eds) *European Lithosphere Dynamics*. Geological Society, London, Memoirs **32**, 579-598.

Downes, H., Peltonen, P., Mänttäri, I. & Sharkov, E.V. (2002). Proterozoic zircon ages from lower crustal granulite xenoliths, Kola Peninsula: evidence for crustal growth and reworking. *Journal of the Geological Society of London* **159**, 485–488

Ewing, T., Rubatto, D. & Hermann, J. (2014). Hafnium isotopes and Zr/Hf of rutile and zircon from lower crustal metapelites (Ivrea–Verbano Zone, Italy): Implications for chemical differentiation of the crust. *Earth and Planetary Science Letters* **389**, 106–118.

Glebovitsky, V.A. (1997). *The Early Precambrian of Russia*. Harwood.

Glebovitskii, V.A., Baltybaev, S.K., Levchenkov, O.A. & Kuzmina, E.V. (2009). Thermodynamic regime of Svecofennian (1.9 Ga) metamorphism of the Umba nappe of the Lapland collisional orogen. *Petrology* **17**, 331-351.

Harley, S.L. & Kelly, N.M. (2007). The impact of zircon–garnet REE distribution data on the interpretation of zircon U–Pb ages in complex high-grade terrains: An example from the Rauer Islands, East Antarctica. *Chemical Geology* **241**, 62–87.

Hoskin, P.W.O. & Schaltegger, U. (2003). The composition of zircon and igneous and metamorphic petrogenesis. In: Hanchar, J.M. & Hoskin, P.W.O. (eds) *Zircon*. Reviews in Mineralogy and Geochemistry **53**, 27-62.

Kempton, P.D., Downes, H., Sharkov, E.V., Vetrin, V.R., Ionov, D.A., Carswell, D.A. & Beard, A. (1995). Petrology and geochemistry of xenoliths from the Northern Baltic Shield: evidence for partial melting and metasomatism in the lower crust beneath an Archaean terrane. *Lithos* **36**, 157-184.

Kempton, P.D., Downes, H., Neymark, L.A., Wartho, J.A., Zartman, R.E. & Sharkov, E.V. (2001). Garnet granulite xenoliths from the Northern Baltic Shield - the underplated lower crust of a Palaeoproterozoic large igneous province? *Journal of Petrology* **42**, 731-763.

Klemme, S., Blundy, J.D. & Wood, B.J. (2002). Experimental constraints on major and trace element partitioning during partial melting of eclogite. *Geochimica et Cosmochimica Acta* **66**, 3109–3123.

Koreshkova, M.Yu., Levsky, L.K. & Ivanikov, V.V. (2001). Petrology of a lower crustal xenolith suite from dykes and explosion pipes of Kandalaksha graben. *Petrology* **9**, 79-96.

Koreshkova, M.Yu., Downes, H., Glebovitsky, V.A., Rodionov, N.V., Antonov, A.V. & Sergeev, S.A. (2014). Zircon trace element characteristics and ages in granulite xenoliths: a key to understanding the age and origin of the lower crust, Arkhangelsk kimberlite province, Russia. *Contributions to Mineralogy and Petrology* **167**, 973.

Kretz, R. (1983). Symbols for rock forming minerals. *American Mineralogist* **68**, 277-279.

Makhotkin, I.L., Gibson, S.A., Thompson, R.N., Zhuravlev, D.Z. & Zherdev, P.U. (2000). Late Devonian diamondiferous kimberlite and alkaline picrite (Proto-kimberlite?) magmatism in the Arkhangelsk region, NW Russia. *Journal of Petrology* **41**, 201-227.

Markwick, A.J.W. & Downes, H. (2000). Lower crustal granulite xenoliths from the Arkhangelsk kimberlite pipes: petrological, geochemical and geophysical results. *Lithos* **51**, 135-151.

Mintz, M.V., Glaznev, V.N., Konilov, A.N., Kunina, N.M., Nikitichev, A.P., Raevsky, A.B., Sedikh, Yu.N., Stupak, V.M. & Fonarev, V.I. (1996). *The Early Precambrian of the Northeastern Baltic Shield: palaeogeodynamics, crustal structure and evolution*. Scientific World, Moscow. (Nauchnii Mir, In Russian)

Nehring, F., Foley, S.F. & Hölttä, P. (2010). Trace element partitioning in the granulite facies. *Contributions to Mineralogy and Petrology* **159**, 493–519.

Nikitina, L.P., Levskii, L.K., Lokhov, K.I., Belyatskii, B.V., Zhuravlev, V.A., Lepekhina, E.V. & Antonov, A.V. (1999). Proterozoic alkaline ultramafic magmatism in the eastern part of the Baltic Shield. *Petrology* **7**, 246-266.

Peltonen, P., Mänttäri, I., Huhmaa, H. & Whitehouse, M.J. (2006). Multi-stage origin of the lower crust of the Karelian craton from 3.5 to 1.7 Ga based on isotopic ages of kimberlite-derived mafic granulite xenoliths. *Precambrian Research* **147**, 107–123.

Reddy, S.M., Timms, N.E., Trimby, P., Kinny, P.D., Buchan, C. & Blake, K. (2006). Crystal-plastic deformation of zircon: A defect in the assumption of chemical robustness. *Geology* **34**, 257–260.

Rubatto, D. & Hermann, J. (2003). Zircon formation during fluid circulation in eclogites (Monviso, Western Alps): Implications for Zr and Hf budget in subduction zones. *Geochimica et Cosmochimica Acta* **67**, 2173–2187.

Rubatto, D. & Hermann, J. (2007). Experimental zircon/melt and zircon/garnet trace element partitioning and implications for the geochronology of crustal rocks. *Chemical Geology* **241**, 38–61

Samsonov, A.V., Nosova, A.A., Tretyachenko, V.V., Larchenko, V.A. & Larionova, Yu.O. (2009). Collisional sutures in the Early Precambrian Crust as a factor responsible for localization of diamondiferous kimberlites in the northern East European Platform. *Doklady Earth Sciences* **424,** 226-230.

Schmitz, M.D. & Bowring, S.A. (2003). Constraints on the thermal evolution of continental lithosphere from U-Pb accessory mineral thermochronometry of lower crustal xenoliths, southern Africa. *Contributions to Mineralogy and Petrology* **144**, 592–618.

Sláma, J., Košler, J. & Pedersen, R.B. (2007). Behaviour of zircon in high-grade metamorphic rocks: Evidence from Hf isotopes, trace elements and textural studies. *Contributions to Mineralogy and Petrology* **154**, 335–356.

Sun, Ch. & Liang, Y. (2015). A REE-in-garnet–clinopyroxene thermobarometer for eclogites, granulites and garnet peridotites. *Chemical Geology* **393-394**, 79–92.

Tuisku, P., Huhma, H. & Whitehouse, M.J. (2012). Geochronology and geochemistry of the enderbite series in the Lapland Granulite Belt: generation, tectonic setting, and correlation of the belt. *Canadian Journal of Earth Sciences* **49**, 1-19.

Van Orman, J.A., Grove, T.L. & Shimizu, N. (2001). Rare earth element diffusion in diopside: influence of temperature, pressure and ionic radius, and an elastic model for diffusion in silicates. *Contributions to Mineralogy and Petrology* **141,** 687-703.

Van Orman, J.A., Grove, T.L., Shimizu, N. & Layne, G.D. (2002) Rare earth element diffusion in a natural pyrope single crystal at 2.8 GPa. *Contributions to Mineralogy and Petrology* **142**, 416-424.

Vavra, G., Schmid, R. & Gebauer, D. (1999). Internal morphology, habit and U-Th-Pb microanalysis of amphibolite-to-granulite facies zircons: geochronology of the Ivrea Zone (Southern Alps). *Contributions to Mineralogy and Petrology* **134**, 380-404.

Vetrin, V.R. & Kalinkin, M.M. (1992). *Reconstruction of processes of intracrustal and crustal-mantle magmatism and metasomatism.* Apatity. (In Russian)

Vetrin, V. R., Lepekhina, E. N., Paderin, I. P. & Rodionov, N. V. (2009). Stages of the Lower Crust Formation of the Belomorian Mobile Belt, Kola Peninsula. *Doklady Earth Sciences* **425**, 269-273.

Vetrin, V. R. & Nemchin, A.A. (1998). The U–Pb Age of Zircon from a Granulite Xenolith in the Diatreme on the Elovyi Island, the Southern Kola Peninsula. *Doklady Earth Sciences* **359A**, 454-456.

Zack, T., Foley, S. & Jenner, G. (1997). A consistent partition coefficient set for clinopyroxene, amphibole and garnet from laser ablation microprobe analysis of garnet pyroxenites from Kakanui, New Zealand. *Neues Jahrbuch Für Mineralogie - Abhandlungen* **172**(1), 23-41.

Zheng, J., Griffin, W.L., O'Reilly, S.Y., Lu, F., Yu, C., Zhang, M. & Li, H. (2004). U-Pb and Hf-isotope analysis of zircons in mafic xenoliths from Fuxian kimberlites: evolution of the lower crust beneath the North China craton. *Contributions to Mineralogy and Petrology* **148**, 79-103.

FIGURE CAPTIONS

Fig. 1. Locality map of the Kandalaksha dike swarm and Arkhangelsk kimberlite province in relation to the regional geology (adapted from Daly *et al*., 2001, 2006). Legend: Archaean granite-gneiss areas (1); Late Archaean Belomorian mobile belt (B) (2); Early Proterozoic Svecofennian complexes (3); Early Proterozoic volcanosedimentary complexes (4); Early Proterozoic Lapland-Kolvitza mobile belt (LK) (5); Neoproterozoic-Paleozoic sedimentary cover (6); geological boundaries (7); dikes and pipes of Kandalaksha and the Grib pipe in the Arkhangelsk kimberlite province (8).

Fig. 2. CL images of zircons. Spot numbers and $^{207}Pb/^{206}Pb$ ages (Ma) are shown. Scale bar is the same for all images.

Fig. 3. REE patterns of zircons from Grt-granulites. Dashed lines indicate calculated compositions of zircon in equilibrium with garnet ($D^{Zrn/Grt}$ from Rubatto & Hermann (2007)). Values are normalized to chondrite (Sun & McDonough, 1989).

Fig. 4. REE patterns of zircons and garnets from Grt-websterite Mk459, eclogite Mk284 and Grt-Phl-rocks Mk540 and Mk172. Values are normalized to chondrite (Sun & McDonough, 1989).

Fig. 5. U-Pb concordia diagrams for zircon from lower crustal xenoliths from the Grib kimberlite pipe. Error ellipses are 2σ. Decay constant errors are included. Colors for ellipses as in Figs 3 and 4.

Fig. 6. εHf(t) vs U-Pb zircon age. Dashed lines are Pb-loss trajectories.
DM – Depleted Mantle; CHUR – Chondritic Uniform Reservoir

Fig. 7. Traverses across garnet grains from xenoliths from dikes and pipes of the Kandalaksha and Arkhangelsk provinces. Mg number is Mg/(Mg+Fe), f.u., X_{Ca} is Ca/(Fe+Mn+Mg+Ca), f.u.

Fig. 8. Variation of Zr contents in garnet, clinopyroxene and rutile. (a) Zr content in garnet *vs* Zr content in clinopyroxene. Lines correspond to $D^{Grt/Cpx} = 0.1$, 0.2, 0.3 and 0.4; (b) Zr content in rutile *vs* Zr content in clinopyroxene; (c) Zr content in rutile *vs* Zr content in garnet.

Fig. 9. Initial $^{176}Hf/^{177}Hf$ *vs* age plots for zircons from Grt-granulites Mk111 (a) and 77/690 (b) and whole-rock samples N55 and N39, and schematic relationship with mineral associations. Solid diamonds are for CL-dark sector-zoned cores from Mk111. Other symbols are as in Fig. 6.

Fig. 10. Summary of garnet and zircon relationships

Table 1. Modal mineralogy (vol.%) and P-T determinations for Kola xenoliths.

sample	texture	Grt	Opx	Cpx	Pl	Kfs	Qtz	Prg	Phl	Rt	Ilm	Ap	Scp	Secondary minerals	T core, °C	P core, GPa	T rim, °C	P rim, GPa	T Zr-in-Rt, °C
Mk111	c/g, banded, p/b	37		30	24		8			0.1	0.3	0.2		1	800	1.3	680	1.2	890
Mk260	c/g, foliated, p/b	25	13	39	17			4	1	0.2	0.3	0.2		1	660	1.1	550	1.0	910
Mk325	c/g, banded, p/b	33		17	33	15				0.8	x	1.0		x	710	1.3	670	1.3	
Mk326	c/g, banded, p/b	21		18	45	5			1	1.2	x	0.9	3.0	5	770	1.4	635	1.2	860
Mk523	c/g, foliated, p/b	23		27	45		3			0.6	0.2	0.6	0.2	x	790	1.5	570	1.2	870
Mk459	c/g, foliated, p/b	36	7	56						0.4		0.6		x	610	1.4[a]	550	1.2[a]	890
Mk284	c/g, foliated, p/b	34		33				8	23	0.8	x	0.8		x	720	1.4[b]	620	1.4[b]	640
Mk172	c-m/g, foliated, p/b	5							95		x			x					
Mk540	c/g, foliated, p/b	39	27						33	1.0	x			x				0.9[a,c]	700
Mk536	c-m/g, foliated, g/b			69				3	28					x					

Abbreviations: m/g – medium-grained, c/g –coarse-grained, g/b – granoblastic, p/b – porphyroblastic, x - < 0.5 vol.%.
Mineral symbols are according to Kretz (1983).
T – temperature estimate using the Grt-Cpx geothermometer of Ravna (2000), T Zr-in-Rt - using the Zr-in-rutile geothermometer of Watson *et al*. (2006).
P – pressure estimate using the Grt-Pl-Cpx-Qtz geobarometer of Newton & Perkins (1982) for granulites and the Grt-Opx geobarometer of Nickel & Green (1985) (modified version by Taylor (1998)) for pyroxenites.
The calculations were made for grain core and rim compositions, corrected for calculated Fe^{3+} content.
[a] – pressure estimated using Grt-Opx geobarometer (Taylor, 1998)
[b] – assumed pressure
[c] – calculated at $T=T_{Zr\text{-}in\text{-}Rt}$

Table 2. Summary table of zircon compositions from Kola xenoliths.

Sample	Zircon texture	Inclusions/ conjunctions	Ce, ppm	Ce/Ce*	Eu/Eu*	Yb_N/Dy_N	Σ Tb-Lu, ppm	Y, ppm	Th, ppm	U, ppm	Th/U	Th, ppm	U, ppm	Th/U	HfO_2, wt%	calculated Yb_N/Dy_N in Grt at a given T,°C	Measured Yb_N/Dy_N in Grt
												SHRIMP data					
Mk111	CL-dark polygonal sector zoning		4.06	59	0.77	0.4	10	25.9	67.9	476	0.14	64.1	559	0.12	1.40		
	Fir-tree sector zoning	Opx, Pl, Ap	35.1	33	0.29	2.1	277	477	382	143	2.67	316	101	3.21	1.42		
	Homogeneous		10.6	76	0.39	2.6	59	102	50.2	31.4	1.60	48.6	42.4	1.15	1.37		
	Convoluted overgrowths		15.9	114	0.62	1.9	22	45.2	298	82.1	3.63	381	59.1	6.67	1.30	0.8, 950°C	1.0 core - 0.8 rim
	CL-dark rims		30.8	41	0.35	2.4	205	346	276	124	2.22	381	59.1	6.67	1.42		
Mk260	CL-dark polygonal sector zoning		1.05	≥8	0.89	3.0	40	77.2	14.4	518	0.03	91.0	604	0.15	1.35		
	Sector-zoned overgrowths	Grt	4.23	19	0.56	1.4	32	76.4	96.2	226	0.43	80.9	211	0.38	1.30	0.7, 950-1000°C	1.2 core - 1.1 rim
Mk325	Patchy to homogeneous											34.8	47.1	0.70			
Mk326	Sector zoning		17.8	36	0.63	7.5	350	413	115	144	0.80	85.5	168	0.51	1.30		
	CL-dark sectors		26.6	27	0.60	5.6	876	861	357	277	1.29	246	231	1.07	1.31		
	Fir-tree sector zoning	Kfs, Phl	30.6	64	1.10	0.6	27	70.9	127	138	0.92	108	159	0.70	1.10		
	Homogeneous		17.2	16	0.70	2.1	52	94.8	38.2	32.8	1.16	27.7	26.0	1.12	1.30	0.9, 900°C	1.0 core - 0.9 rim
Mk523	Sector zoning		39.2	151	0.66	0.5	26	65.8	235	99.0	2.37	158	74.8	2.11	0.94	0.2, 800-1000°C	0.9 core - 0.8 rim
	Homogeneous	Pl	22.5	184	0.71	0.6	14	35.3	90.3	44.6	2.03	69.7	38.2	1.88	0.87		
	CL-dark rim		57.5	103	0.64	0.4	40	94.7	257	147	1.75	98.4	53.3	1.85	1.05		
Mk459	Sector zoning	Rt, Grt, Cpx	34.6	26	0.34	0.7	27	58.0	236	86.1	2.74	212	76.7	2.76	0.96		0.6 core - 0.6 rim
Mk284	Homogeneous	Rt, Grt, Phl	14.8	28	0.97	0.8	7	17.4	10.3	12.6	0.81	10.4	14.0	0.75	0.72		0.8 core - 0.7 rim
Mk172	Faint sector zoning	Phl	20.0	29	0.62	0.6	4	9.74	47.6	460	0.10	30.0	482	0.06	1.49		1.0 core - 0.9 rim
Mk540	Blurred sector zoning	Phl	30.5	14	0.51	1.1	23	44.9		220	0.42				1.60		1.2 core - 1.1 rim
Mk536	Sector zoning	Phl	9.68	≥47	0.87	3.5	28	46.4		43.5	1.03				1.08		

Table 3. Hf isotopes in zircons, zircon standards and whole rocks.

sample	spot	location	texture	$^{176}Lu/^{177}Hf$	±2SE	$^{176}Hf/^{177}Hf$	±2SE	$^{176}Yb/^{177}Hf$	±2SE	Age (Ma)	SHRIMP spot	$^{176}Hf/^{177}Hf(i)$	εHf(t)	σ	T_{DM} (Ga)
60/473	1	core	sector	0.00040	0.00000	0.281000	0.000027	0.01603	0.00038	2746	3.1.	0.280979	-0.8	0.7	3.04
(Arkh.)	2	interm.	osc.	0.00033	0.00000	0.280957	0.000025	0.01304	0.00026	2715	3.2.	0.280939	-2.9	0.6	3.09
	3	core	sector	0.00046	0.00001	0.280987	0.000030	0.01583	0.00008	1948	4.1.	0.280970	-19.9	0.8	3.06
	4	interm.	osc.	0.00052	0.00000	0.280970	0.000031	0.02025	0.00029	1882	4.2.	0.280951	-22.1	0.8	3.09
	5	rim	hom.	0.00019	0.00000	0.280956	0.000036	0.00740	0.00012	1857	5.1.	0.280949	-22.7	0.9	3.08
	6	core	osc.	0.00064	0.00002	0.280954	0.000020	0.02441	0.00164	2720	CA	0.280921	-3.5	0.5	3.12
	7	core	osc.	0.00079	0.00003	0.280948	0.000030	0.02716	0.00149	2617	6.1.	0.280908	-6.4	0.8	3.14
	8	core	sector	0.00069	0.00001	0.280989	0.000041	0.02283	0.00023	2720	CA	0.280953	-2.3	1.0	3.08
	9	interm.	osc.	0.00091	0.00001	0.280913	0.000027	0.03485	0.00085	2723	2.1.	0.280865	-5.4	0.7	3.20
	10	rim	hom.	0.00015	0.00000	0.280913	0.000032	0.00579	0.00010	1873	1.1.	0.280908	-23.8	0.8	3.14
	11	core	osc.	0.00063	0.00001	0.280977	0.000031	0.02374	0.00057	2346	1.2.	0.280949	-11.3	0.8	3.09
	12	rim	hom.	0.00015	0.00000	0.280938	0.000025	0.00562	0.00008	1805	CA	0.280933	-24.5	0.6	3.10
	13	core	sector	0.00060	0.00001	0.280927	0.000035	0.02008	0.00061	2720	CA	0.280896	-4.4	0.9	3.15
	14	interm.	osc.	0.00041	0.00000	0.281020	0.000029	0.01520	0.00014	2540	7.1.	0.281000	-4.9	0.7	3.01
	15	rim	hom.	0.00023	0.00000	0.280957	0.000038	0.00870	0.00003	1846	7.2.	0.280949	-23.0	1.0	3.08
	16	core	osc.	0.00051	0.00000	0.280952	0.000026	0.01848	0.00027	2720	CA	0.280925	-3.3	0.7	3.11
	17	interm.	CL-dark	0.00042	0.00000	0.280980	0.000031	0.01552	0.00019	2615	8.1.	0.280959	-4.6	0.8	3.07
	18	rim	hom.	0.00001	0.00000	0.281086	0.000041	0.00058	0.00001	1769	9.1.	0.281086	-19.9	1.0	2.90
P5/354	19	core	CL-br.s.	0.00061	0.00000	0.281238	0.000038	0.02543	0.00031	1864	2.1.	0.281216	-13.1	1.0	2.74
(Arkh.)	20	core	hom.	0.00001	0.00000	0.281219	0.000022	0.00059	0.00001	1820	CA	0.281219	-14.0	0.6	2.72
	21	core	hom.	0.00001	0.00000	0.281235	0.000024	0.00058	0.00001	1820	CA	0.281235	-13.4	0.6	2.70
	22	ovegr.	conv.	0.00001	0.00000	0.281268	0.000028	0.00040	0.00001	1824	3.1.	0.281268	-12.2	0.7	2.66
	23	core	sector	0.00060	0.00005	0.281283	0.000033	0.02216	0.00204	1964	4.1.	0.281261	-9.2	0.8	2.68
	24	rim	CL-br.s.	0.00048	0.00001	0.281214	0.000028	0.01613	0.00027	1950	5.2.	0.281196	-11.8	0.7	2.76
	25	core	sector	0.00078	0.00001	0.281250	0.000024	0.02725	0.00047	1958	8.1.	0.281221	-10.7	0.6	2.73
	26	ovegr.	conv.	0.00001	0.00000	0.281227	0.000030	0.00049	0.00002	1822	6.1.	0.281227	-13.7	0.8	2.71
	27	ovegr.	conv.	0.00001	0.00000	0.281242	0.000020	0.00027	0.00001	1822	6.1.	0.281242	-13.1	0.5	2.69
	28	core	sector	0.00014	0.00000	0.281221	0.000030	0.00555	0.00014	1964	CA	0.281216	-10.7	0.8	2.73
	29	core	sector	0.00010	0.00000	0.281234	0.000036	0.00454	0.00009	1977	7.1.	0.281230	-9.9	0.9	2.71
	30	core	sector	0.00092	0.00001	0.281272	0.000026	0.03366	0.00017	1964	CA	0.281237	-10.0	0.7	2.71
77/690	31	core	sector	0.00013	0.00000	0.280934	0.000023	0.00477	0.00006	1826	1.1.	0.280930	-24.1	0.6	3.11
(Arkh.)	32	interm.	CL-br.s.	0.00002	0.00000	0.281113	0.000032	0.00109	0.00001	1825	1.2.	0.281112	-17.7	0.8	2.86
	33	ovegr.	conv.	0.00008	0.00000	0.281406	0.000030	0.00301	0.00006	1815	1.3	0.281403	-7.6	0.8	2.48

Table 3. Continued.

sample	spot	location	texture	$^{176}Lu/^{177}Hf$	±2SE	$^{176}Hf/^{177}Hf$	±2SE	$^{176}Yb/^{177}Hf$	±2SE	Age, Ma	SHRIMP spot	$^{176}Hf/^{177}Hf(i)$	εHf(t)	σ	T_{DM}, Ga
	34	ovegr.	conv.	0.00015	0.00000	0.281317	0.000030	0.00564	0.00012	1836	CA	0.281312	-10.3	0.8	2.60
	35	ovegr.	conv.	0.00008	0.00000	0.281375	0.000039	0.00296	0.00003	1837	2.1.	0.281372	-8.2	1.0	2.52
	36	core	sector	0.00005	0.00000	0.280972	0.000033	0.00206	0.00004	1836	CA	0.280970	-22.4	0.8	3.05
	37	interm.	CL-br.s.	0.00004	0.00000	0.281228	0.000039	0.00168	0.00002	1836	CA	0.281226	-13.4	1.0	2.71
Mk111	1	core	fir-tree	0.00004	0.00000	0.281271	0.000029	0.00192	0.00001	1918	CA	0.281270	-9.9	0.7	2.65
(Kola)	2	core	patchy	0.00001	0.00000	0.281279	0.000028	0.00062	0.00001	1759	CA	0.281279	-13.3	0.7	2.64
	3	core	CL-dark s.	0.00003	0.00000	0.281225	0.000027	0.00142	0.00002	1759	CA	0.281224	-15.2	0.7	2.71
	4	rim	patchy	0.00001	0.00000	0.281284	0.000024	0.00068	0.00001	1759	CA	0.281284	-13.1	0.6	2.63
	5	core	fir-tree	0.00000	0.00000	0.281248	0.000018	0.00017	0.00001	1918	CA	0.281248	-10.7	0.8	2.68
	6	core	CL-dark s.	0.00001	0.00000	0.281220	0.000030	0.00028	0.00002	2252	111-1	0.281220	-3.9	0.8	2.72
	7	core	fir-tree	0.00001	0.00000	0.281286	0.000036	0.00063	0.00002	1918	CA	0.281286	-9.3	0.9	2.63
	8	core	CL-dark s.	0.00001	0.00000	0.281240	0.000019	0.00026	0.00001	1859	CA	0.281240	-12.3	0.5	2.69
	9	core	CL-dark s.	0.00000	0.00000	0.281213	0.000032	0.00017	0.00001	1859	CA	0.281213	-13.3	0.8	2.73
	10	core	fir-tree	0.00009	0.00000	0.281251	0.000032	0.00418	0.00024	1918	CA	0.281248	-10.7	0.8	2.68
	16	rim	CL-dark r	0.00002	0.00000	0.281246	0.000030	0.00084	0.00002	1759	CA	0.281245	-14.5	0.8	2.69
	17	core	hom.	0.00002	0.00000	0.281259	0.000028	0.00127	0.00002	1859	CA	0.281258	-11.7	0.7	2.67
	18	core	hom.	0.00008	0.00001	0.281280	0.000030	0.00368	0.00020	1859	CA	0.281277	-11.0	0.8	2.64
	19	core	fir-tree	0.00011	0.00000	0.281234	0.000033	0.00534	0.00012	1918	CA	0.281230	-11.3	0.8	2.71
	20	rim	patchy	0.00006	0.00000	0.281224	0.000030	0.00293	0.00001	1759	CA	0.281222	-15.3	0.8	2.72
	21	core	patchy	0.00007	0.00000	0.281248	0.000033	0.00318	0.00004	1759	CA	0.281246	-14.5	0.8	2.69
	22	core	patchy	0.00007	0.00000	0.281266	0.000026	0.00355	0.00004	1759	CA	0.281264	-13.8	0.7	2.66
	23	core	fir-tree	0.00009	0.00000	0.281283	0.000033	0.00463	0.00010	1918	CA	0.281280	-9.6	0.8	2.64
	24	core	CL-dark s.	0.00006	0.00000	0.281227	0.000024	0.00256	0.00004	1918	CA	0.281225	-11.5	0.6	2.71
	25	core	fir-tree	0.00001	0.00000	0.281283	0.000025	0.00065	0.00002	1918	CA	0.281282	-9.5	0.6	2.64
	26	ovegr.	conv.	0.00002	0.00000	0.281261	0.000039	0.00110	0.00001	1759	CA	0.281260	-13.9	1.0	2.67
Mk326	8	core	sector	0.00071	0.00000	0.281499	0.000034	0.02824	0.00047	1771	CA	0.281475	-6.0	0.9	2.39
(Kola)	9	core	sector	0.00032	0.00000	0.281469	0.000027	0.01229	0.00017	1640	CA	0.281459	-9.6	0.7	2.41
	10	rim	hom.	0.00002	0.00000	0.281495	0.000027	0.00078	0.00003	1640	CA	0.281494	-8.4	0.7	2.35
	11	core	sector	0.00031	0.00000	0.281480	0.000027	0.01196	0.00025	1771	CA	0.281469	-6.2	0.7	2.39
	12	core	fir-tree	0.00001	0.00000	0.281445	0.000026	0.00067	0.00001	1640	CA	0.281445	-10.2	0.7	2.42
	13	core	sector	0.00065	0.00000	0.281489	0.000031	0.02560	0.00036	1771	CA	0.281467	-6.3	0.8	2.40
	14	core	sector	0.00033	0.00001	0.281503	0.000035	0.01277	0.00039	1771	CA	0.281492	-5.4	0.9	2.36

Table 3. Continued.

sample	spot	location	texture	$^{176}Lu/^{177}Hf$	±2SE	$^{176}Hf/^{177}Hf$	±2SE	$^{176}Yb/^{177}Hf$	±2SE	Age, Ma	SHRIMP spot	$^{176}Hf/^{177}Hf(i)$	εHf(t)	σ	T_{DM}, Ga
	15	core	fir-tree	0.00000	0.00000	0.281471	0.000029	0.00030	0.00001	1640	CA	0.281471	-9.2	0.7	2.39
Mk523	1	core	sector	0.00000	0.00000	0.281468	0.000025	0.00028	0.00001	1740	CA	0.281468	-7.0	0.6	2.39
(Kola)	2	rim	sector	0.00001	0.00000	0.281454	0.000039	0.00037	0.00001	1740	CA	0.281454	-7.5	1.0	2.41
	3	core	sector	0.00001	0.00000	0.281470	0.000038	0.00041	0.00002	1740	CA	0.281470	-6.9	1.0	2.39
	4	core	sector	0.00001	0.00000	0.281470	0.000039	0.00044	0.00002	1740	CA	0.281470	-6.9	1.0	2.39
	5	rim	CL-dark r	0.00001	0.00000	0.281444	0.000036	0.00054	0.00001	1740	CA	0.281444	-7.9	0.9	2.42
	6	rim	CL-dark r	0.00001	0.00000	0.281446	0.000028	0.00044	0.00001	1740	CA	0.281446	-7.8	0.7	2.42
	7	core	hom.	0.00001	0.00000	0.281499	0.000045	0.00038	0.00002	1740	CA	0.281499	-5.9	1.1	2.35
Mk459	1	core	sector	0.00001	0.00000	0.281486	0.000049	0.00046	0.00003	1700	Zr1.2.	0.281486	-7.3	1.2	2.37
Mk172	2	core	sector	0.00000	0.00000	0.281288	0.000033	0.00007	0.00001	1653	Zr2.1.	0.281288	-15.4	0.8	2.63
Mk172	3	core	sector	0.00000	0.00000	0.281274	0.000047	0.00007	0.00001	1661	Zr2.2.	0.281274	-15.7	1.2	2.65
Mk284	4	core	hom.	0.00001	0.00000	0.281346	0.000040	0.00049	0.00001	1651	Zr3.1.	0.281346	-13.4	1.0	2.55
Mk284	5	rim	hom.	0.00001	0.00000	0.281380	0.000040	0.00037	0.00002	1271	Zr3.4.	0.281380	-21.0	1.0	2.51
91500				0.00029	0.00001	0.282290	0.000024								
Mud Tank				0.00001	0.00000	0.282479	0.000019								
N27-21		wr		0.01265	0.00000	0.281871	0.000004	0.00002	0.00000	2720		0.281206	6.7	0.1	2.75
N39		wr		0.02199	0.00000	0.282201	0.000008	0.00006	0.00001	2720		0.281045	0.9	0.2	3.26
N41-7		wr		0.00716	0.00000	0.281549	0.000004	0.00001	0.00000	2720		0.281172	5.5	0.1	2.80
N43		wr		0.01850	0.00000	0.281924	0.000004	0.00002	0.00000	2720		0.280951	-2.4	0.1	3.40
N55		wr		0.02201	0.00000	0.282243	0.000004	0.00000	0.00000	2720		0.281086	2.4	0.1	3.13

Abbreviations: Arkh. - Arkhangelsk, interm. - intermediate shell, ovegr. - overgrowth, wr - bulk rock analysis, sector – sector-zoning, osc. – oscillatory zoning, hom. – homogeneous, CL-dark s. - CL-dark sector-zoning, CL-br. s. - CL-bright sector-zoning (ghost texture), fir-tree - fir-tree sector-zoning, conv. – convoluted, CL-dark r - CL-dark outer rim, CA - Concordia age.

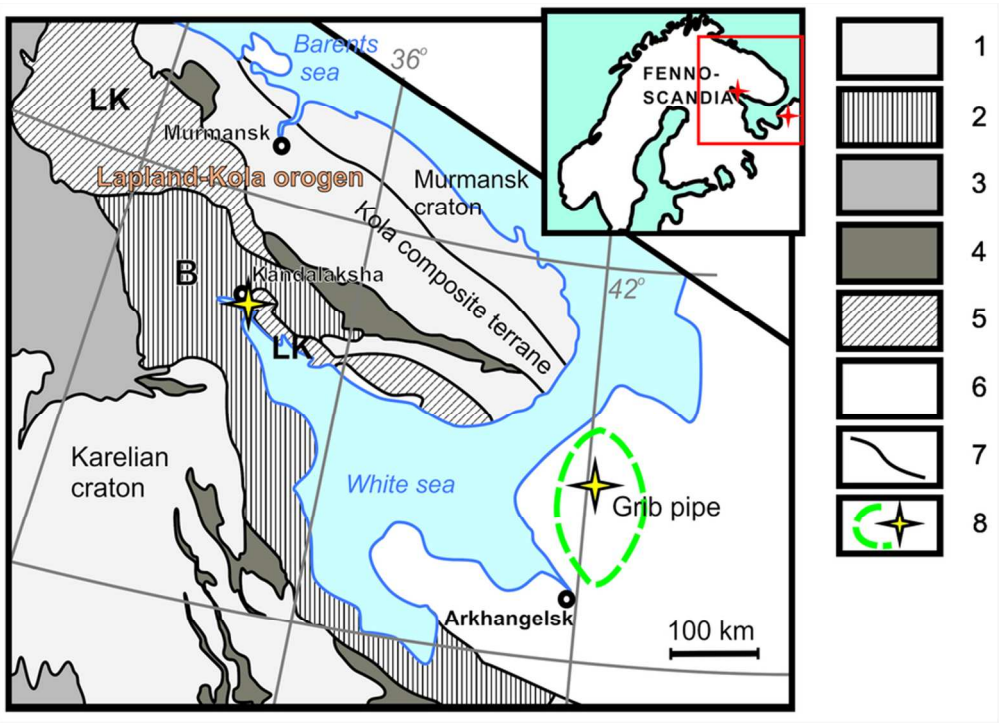

Fig. 1. Locality map of Kandalaksha dike swarm and Arkhangelsk kimberlite province in relation to regional geology (adapted from Daly et al., 2001, 2006). Legend: Archaean granite-gneiss areas (1), Late Archaean Belomorian mobile belt (B) (2), Early Proterozoic Svecofennian complexes (3), Early Proterozoic volcanosedimentary complexes (4), Early Proterozoic Lapland-Kolvitza mobile belt (LK) (5), Neoproterozoic-Paleozoic sedimentary cover (6), geological boundaries (7), dikes and pipes of Kandalaksha and the Grib pipe in Arkhangelsk kimberlite province (8).

82x59mm (300 x 300 DPI)

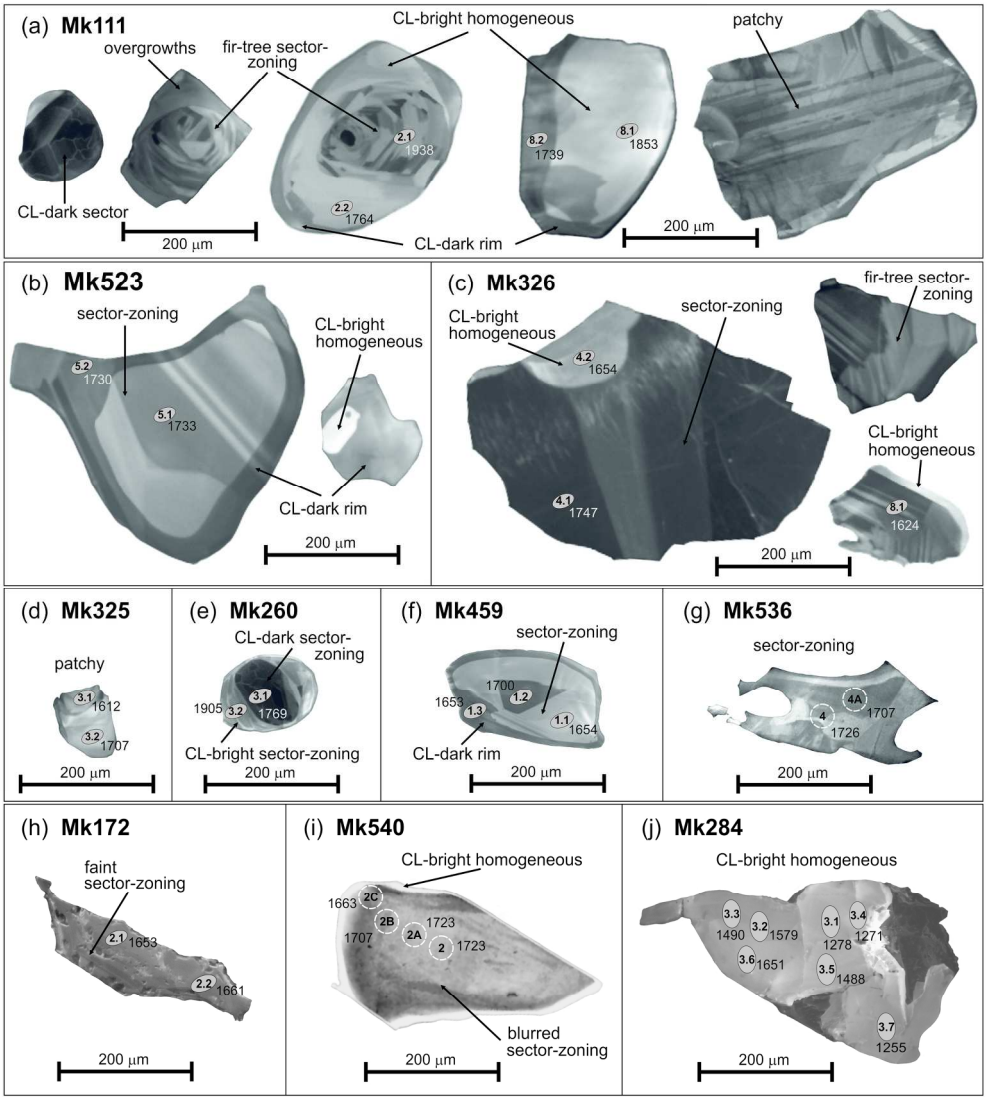

Fig. 2. CL images of zircons. Spot numbers and $^{207}Pb/^{206}Pb$ ages (Ma) are shown. Scale bar is the same for all images.

199x223mm (300 x 300 DPI)

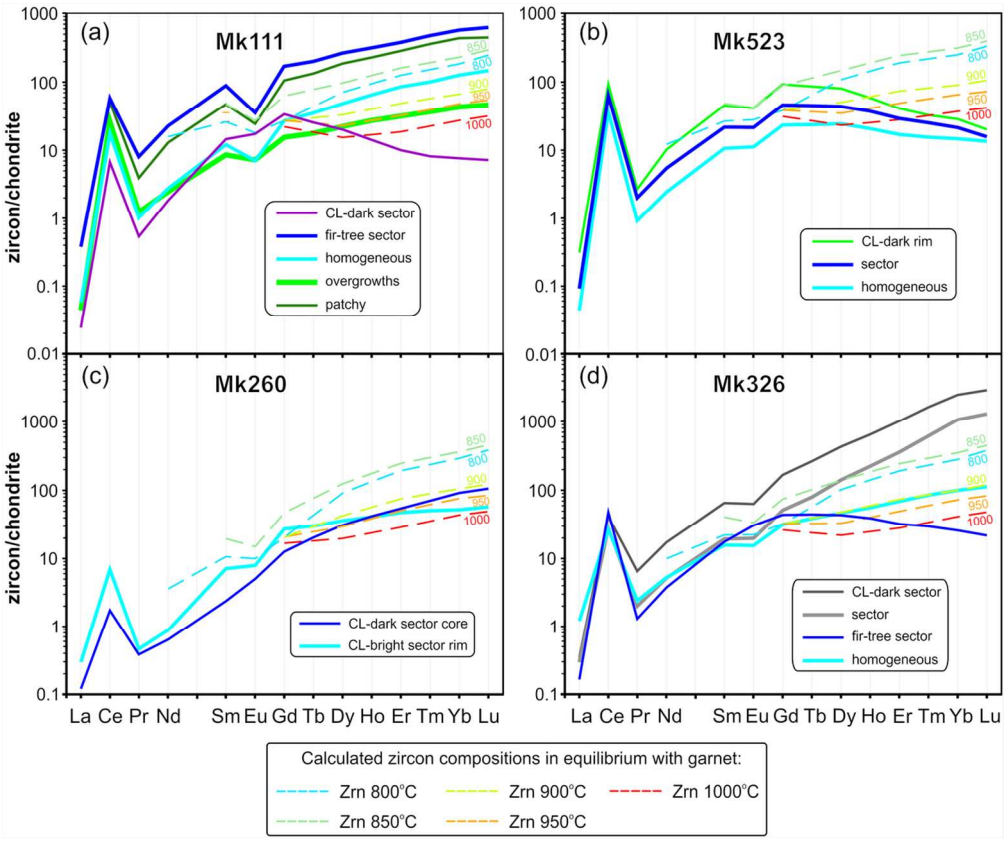

Fig. 3. REE compositions of zircons from Grt-granulites. Dashed lines present calculated compositions of zircon in equilibrium with garnet ($D^{Zrn/Grt}$ are from Rubatto and Hermann (2007)). Values are normalized to chondrite (Sun & McDonough, 1989).

116x97mm (300 x 300 DPI)

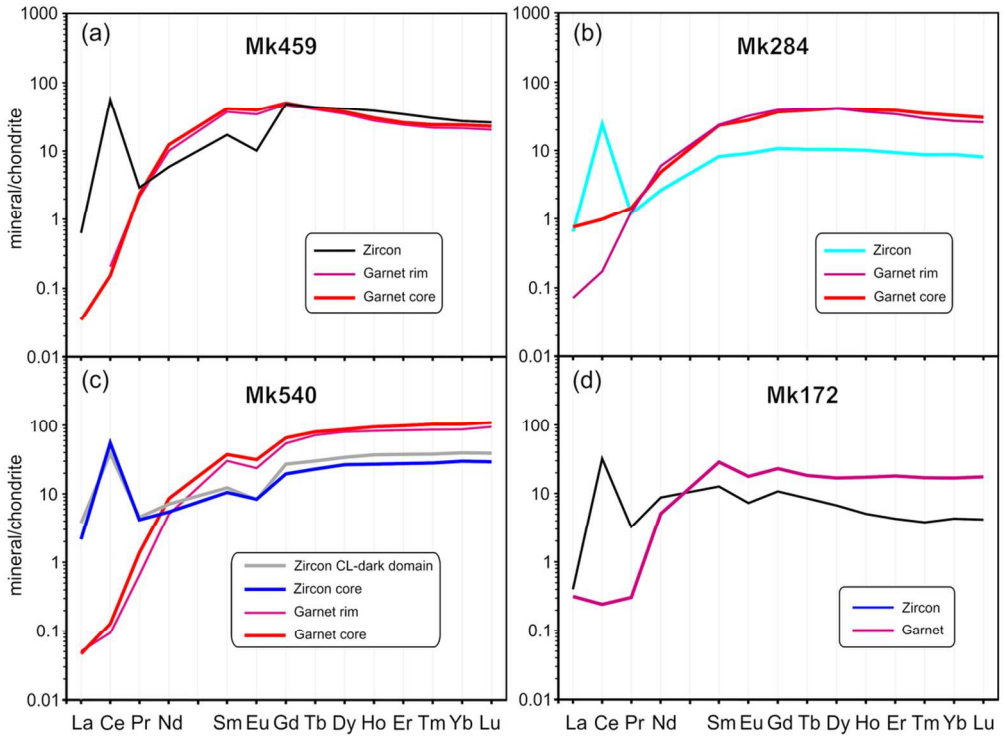

Fig. 4. REE compositions of zircons and garnets from Grt-websterite Mk459, eclogite Mk284 and Grt-Phl-rocks Mk540 and Mk172. Values are normalized to chondrite (Sun & McDonough, 1989).

105x77mm (300 x 300 DPI)

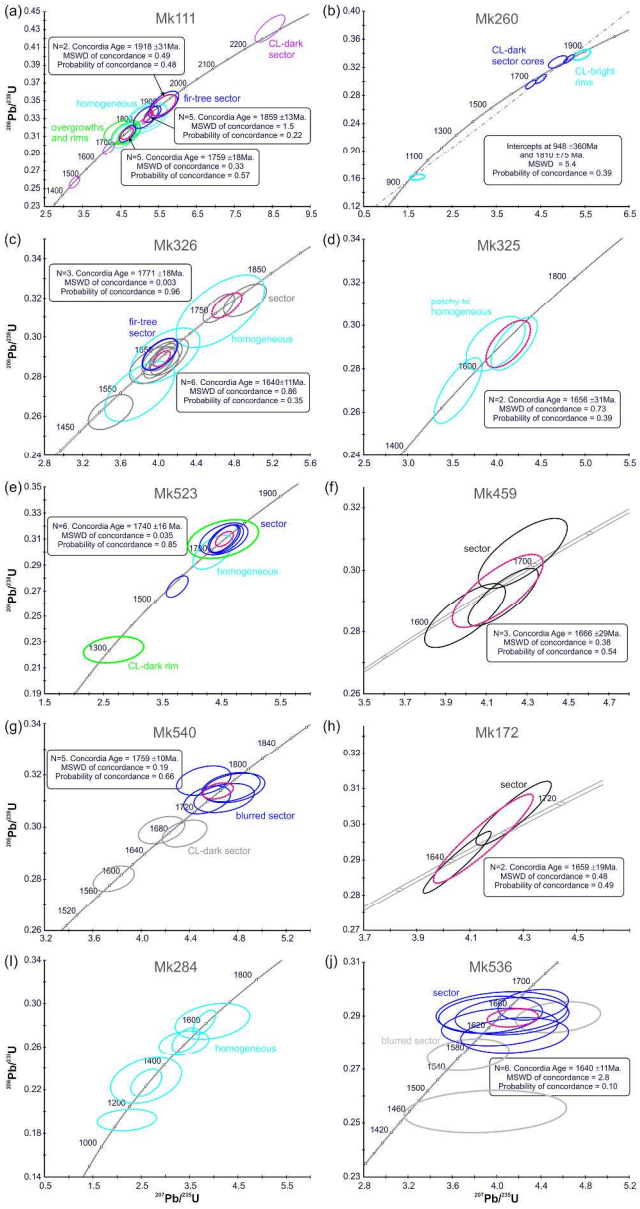

Fig. 5. U-Pb concordia diagrams for zircon data from lower crustal xenoliths from the Grib kimberlite pipe. Data-point error ellipses are 2σ. Decay constants errors are included. Colors for ellipses as for Figures 3 and 4.

212x398mm (300 x 300 DPI)

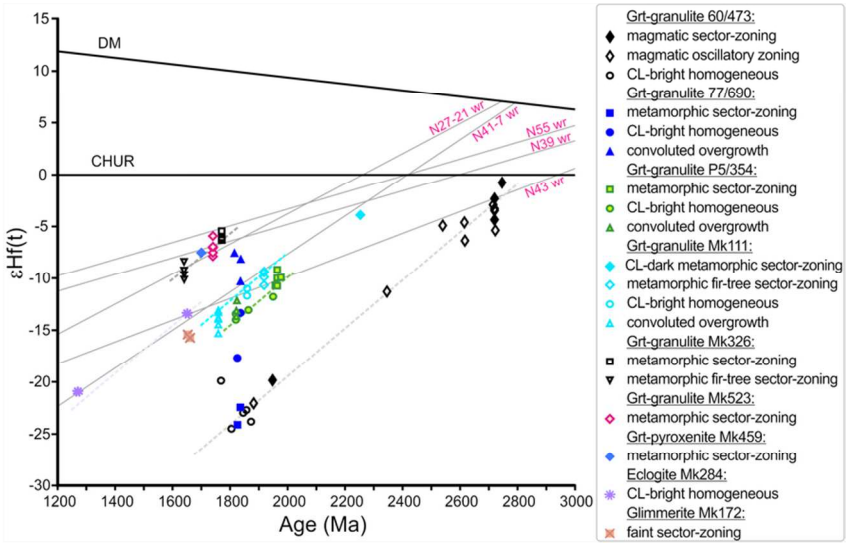

Fig. 6. Plot of εHf(t) vs U-Pb zircon age. Dashed lines are Pb-loss trajectories.

89x48mm (300 x 300 DPI)

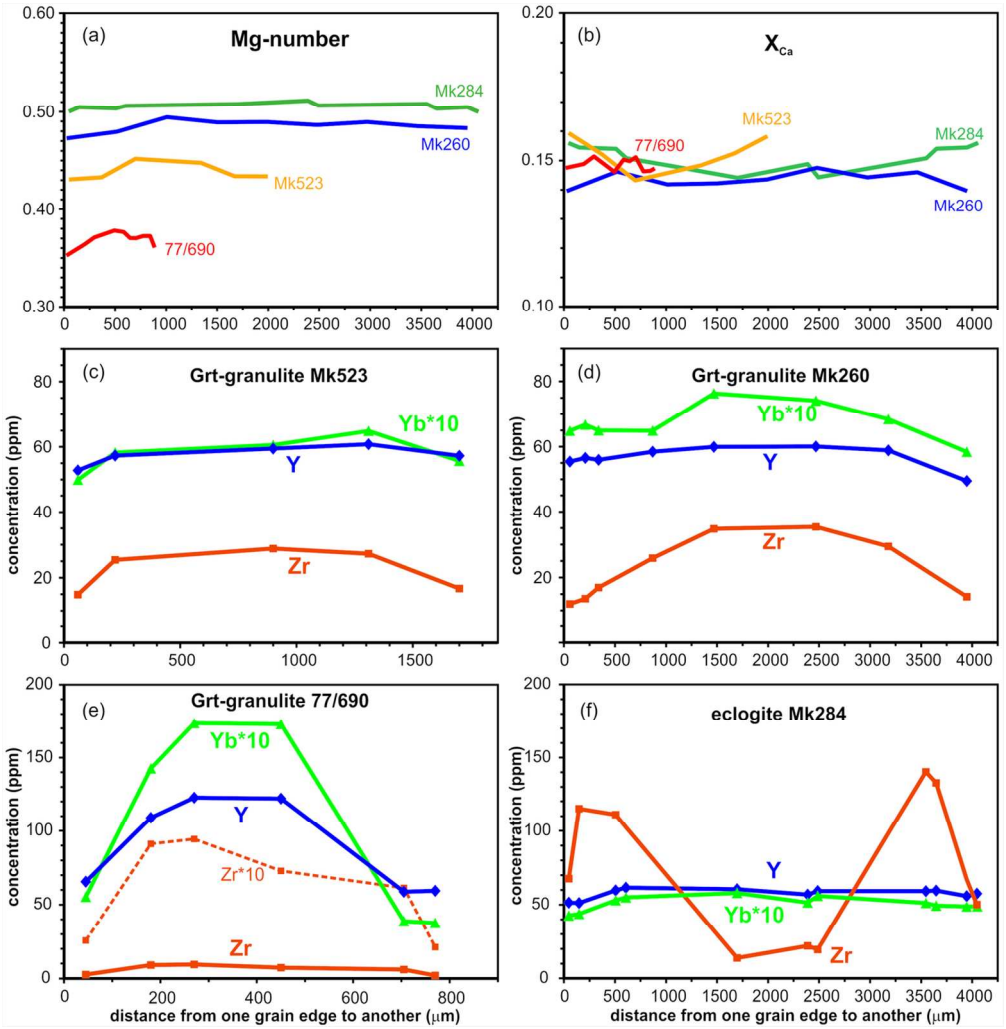

Fig. 7. Traverses across garnet grains from xenoliths from dikes and pipes of Kandalaksha and Arkhangelsk provinces. Mg number is Mg/(Mg+Fe), f.u., X_{Ca} is Ca/(Fe+Mn+Mg+Ca), f.u.

120x123mm (300 x 300 DPI)

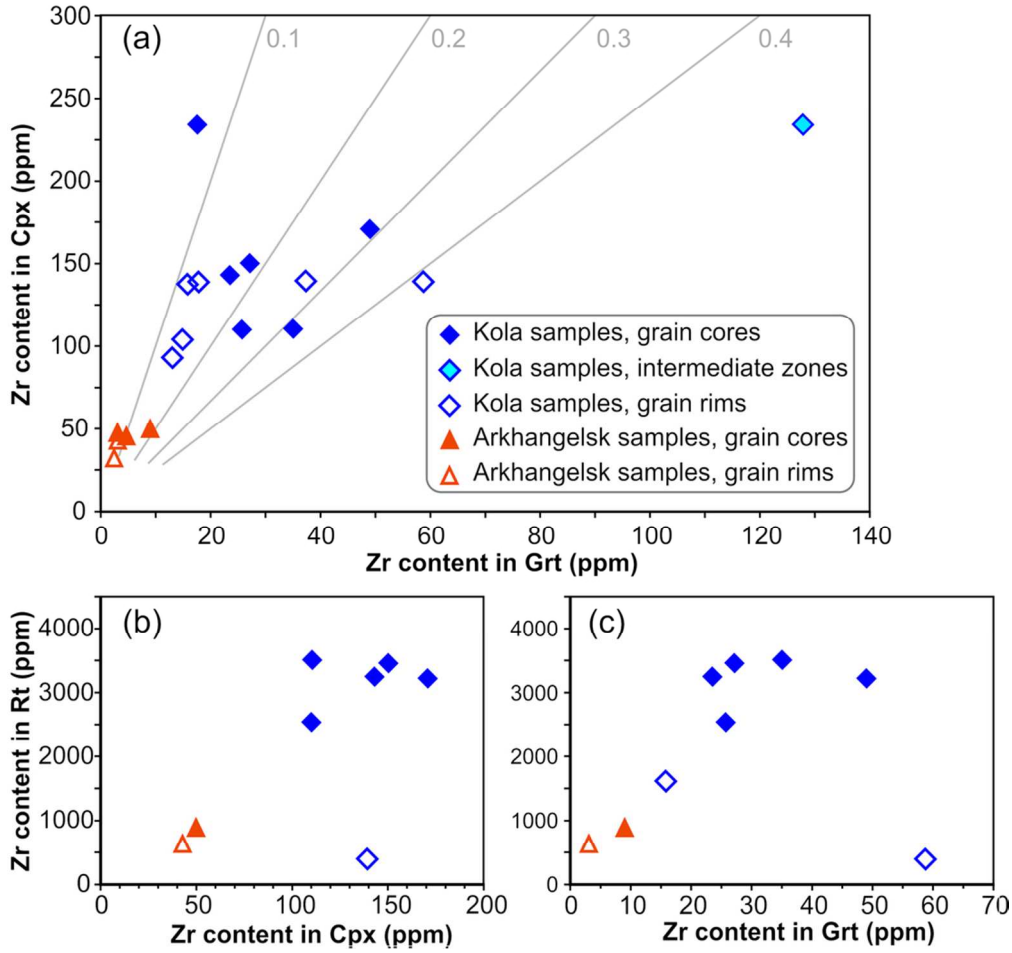

Fig. 8. Plots of Zr contents in garnet, clinopyroxene and rutile. (a) Zr content in garnet vs Zr content in clinopyroxene. Lines correspond to $D^{Grt/Cpx}$ = 0.1, 0.2, 0.3 and 0.4; (b) Zr content in rutile vs Zr content in clinopyroxene; (c) Zr content in rutile vs Zr content in garnet.

93x88mm (300 x 300 DPI)

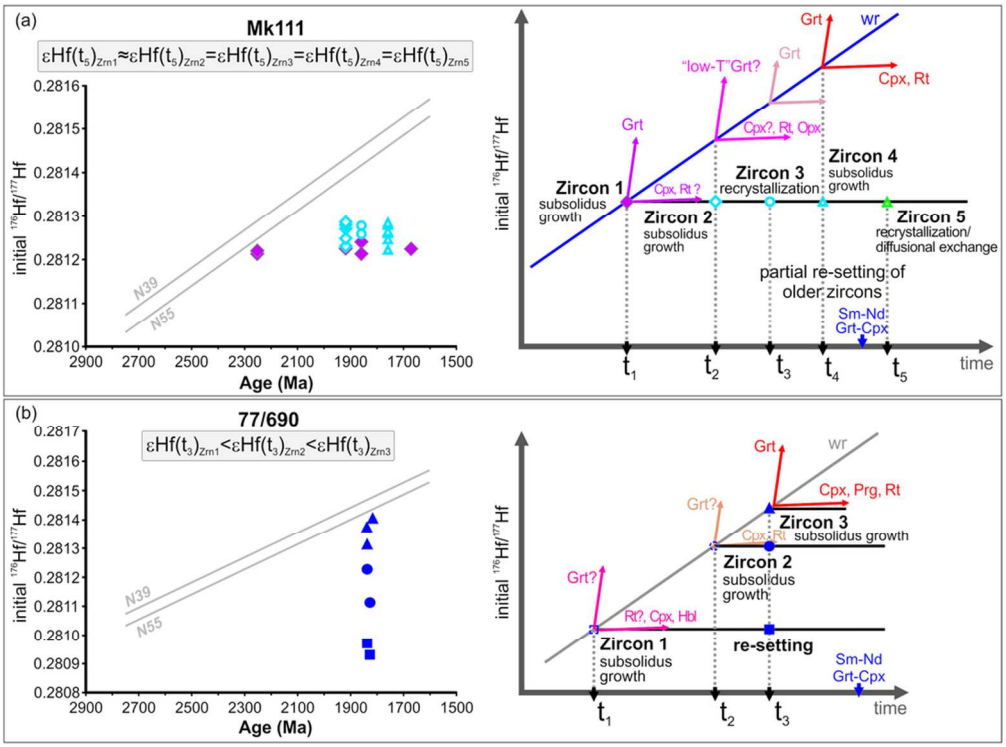

Fig. 9. Initial $^{176}Hf/^{177}Hf$ vs age plots for zircons from Grt-granulites Mk111 (a) and 77/690 (b) and whole rock samples N55 and N39, and schematic relationship with mineral associations. Solid diamonds are for CL-dark sector-zoned cores from Mk111. Other symbols are as for Figure 6.

92x68mm (300 x 300 DPI)

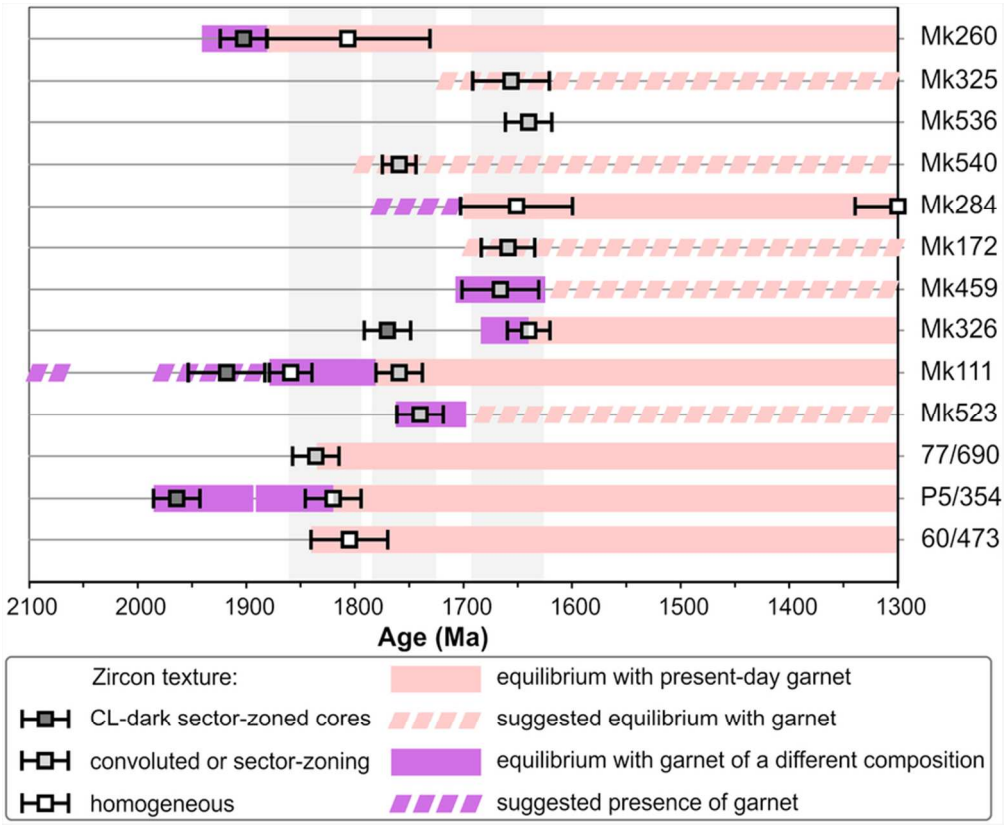

Fig. 10. Summary of garnet and zircon relationship

77x63mm (300 x 300 DPI)